RT NO 5 - GALCIT 101
ontract No. RU-293
October 1, 1959 - December 31, 1959

FUNDAMENTAL STUDIES RELATING TO SYSTEMS ANALYSIS OF SOLID PROPELLANTS

15 January 1960

Guggenheim Aeronautical Laboratory
California Institute of Technology
Pasadena, California

PROGRESS REPORT NO. 5 - GALCIT 101

Subcontract No. RU-293

October 1, 1959 - December 31, 1959

Fundamental Studies Relating to Systems Analysis of Solid Propellants

15 January 1960

P. J. Blatz
W. G. Knauss
R. A. Schapery
L. D. Stimpson
M. L. Williams

This research is supported by
The Thiokol Chemical Corp., Redstone Division

Guggenheim Aeronautical Laboratory
California Institute of Technology
Pasadena, California

PREFACE

Previous reports of this series have attempted to define some of the important parameters affecting the structural integrity of solid propellant rocket grains. Three general areas have been discussed, namely material properties, analytical procedures, and criteria for mechanical failure.

This particular report is devoted to a more detailed examination of the properties of a filled viscoelastic resin, and their representation by appropriate mechanical models. In addition, a comparison of two methods of computing viscoelastic strains in a pressurized cylinder is presented.

In the category of material properties, linear viscoelastic model theory is reviewed, and certain important relations among sets of experimental data are deduced. A justification for the application of this theory is provided by the analytic representation of available dynamic data in terms of a well-known distribution function. Since the inception of this work additional experimental data on propellants has become available.

In the category of analytical procedures, the usual approach of representing material properties by a four-element model, as determined from the dynamic data in a limited frequency range, is compared with the more sophisticated Fourier transform method in which the entire frequency range is utilized. The two approaches are applied to calculate the viscoelastic hoop strain at the inner boundary of an internally pressurized infinitely long hollow cylinder subjected to a ramp-type pressure pulse. In this example, the dilatation is assumed elastic or frequency independent and the distortion viscoelastic.

In the following quarter, primary effort will be devoted to the determination of a criterion for mechanical failure of propellants. Two steps are involved. One is the analytical representation of ultimate strain as a function of temperature on strain rate by means of a mechanical model. In addition to the usual distribution of relaxation (or retardation) times, this model will be supplied with a distribution of ultimate strain. Step two involves the choice of a suitable criterion for compounding ultimate strain or ultimate stress components into a single parameter, which, when exceeded at a given rate and temperature, denotes the onset of fracture or mechanical failure.

TABLE OF CONTENTS

TABLE OF CONTENTS (Cont'd)

I. MATERIAL BEHAVIOR

A. Model Theory

1. General introduction

In order to predict the strain response of viscoelastic materials to applied stress, it is necessary to know the elastic and viscous parameters of the material as a function of time, rate, and temperature. In principle these parameters may all be combined into a generalized stress-strain law such that the strain (stress) may be calculated or deduced for an applied stress (strain) as a function of these parameters. When it is justified to assume this behavior is of linear form, based upon experimental evidence, one can view this association between stress and strain as a transfer function having the property that when it is multiplied by a linear functional of strain (stress) it generates the associated linear functional of stress (strain).

Illustrations of these relations have been covered in the first two progress reports and it is not intended to reiterate them at this time. As a point of departure however it may be recalled that a spring and dashpot in parallel has been designated a Voigt element (Fig. 5, PR No. 1). If now one generalizes either of the above representations in order to better approximate the actual behavior of the material, two approaches are open. First one may consider essentially parallel array of Maxwell[1] elements which is called a Wiechert model (Fig. 9, PR No. 2), or a series[2] array of Voigt elements called a Kelvin model (Fig. 10, PR No. 2). It develops that if the number of components be increased to infinity, either the Wiechert or Kelvin models are capable of representing the material exactly, and perforce, must themselves be related. Thus while either may be used, as a matter of practical convenience the Wiechert representation is used when determining the stress response due to a specified strain input. Conversely the Kelvin is used to find strains resulting from applied stress.

Conceptually therefore, in either case, one has an infinite number of elastic springs and an infinite number of viscous dashpots. If then one were to describe each ith element by its elastic content m_i and relaxation time τ_i, this would be literally a description of the response behavior of the material. The correlation between elastic constant, m_i, and relaxation time, τ_i, ($i = 1, 2, \ldots \infty$) is called a distribution function. It is easy to

understand that if one could assign a particular distribution function to the model, the material behavior could be approximated, with the degree of accuracy of the approximation depending upon how well the experimental data could be fit. Several distribution functions can be used for this purpose, and in the following sections their relative merits will be discussed.

2. Material representation

a. Relaxation spectrum. As presented in the second progress report the Wiechert model leads to the following operator equation relating stress and strain

$$\sigma(t) = \left[m_e + \int_0^\infty \frac{H(\tau)}{\left(\frac{d}{dt} + \tau\right)} d\ln\tau \, \frac{d}{dt} \right] \epsilon(t) \qquad \text{(I-1)}$$

where the elastic spring constants, m_i, are defined in terms of a relaxation spectrum, $H(\tau)$, as

$$m_i \equiv H(\tau_i) \frac{\Delta_i \tau}{\tau_i} \; ; \quad m_g - m_e = \sum' m_i \qquad \text{(I-2)}$$

and the dashpot viscosities, η_i, are defined

$$\tau_i = \frac{1}{\mu_i} = \eta_i / m_i \qquad \text{(I-3)}$$

In operational form, using the Laplace transform (I-1) is equivalent to

$$\frac{\bar{\sigma}}{\bar{\epsilon}} = m_e + \int_0^\infty \frac{p H(\tau) d\ln\tau}{p + \frac{1}{\tau}} = m_e + \int_0^\infty \frac{p}{p+\mu} \frac{H(\mu)}{\mu} d\mu \qquad \text{(I-4)}$$

b. Retardation spectrum. In a similar fashion the Kelvin model gives

$$\epsilon(t) = \left[L_g + \int_0^\infty \frac{L(\tau) d\tau}{\left(\frac{d}{dt} + \frac{1}{\tau}\right)\tau^2} \right] \sigma(t) \qquad \text{(I-5)}$$

where the inverse spring constants, k_i, are defined in terms of the retardation spectrum, $L(\tau)$, as

$$k_i = L(\tau_i) \frac{\Delta\tau_i}{\tau_i} \qquad \text{(I-6)}$$

and the dashpot fluidities, ϕ_i, are defined

$$\tau_i = \frac{1}{\mu_i} = \frac{k_i}{\phi_i} \; ; \quad k_e - k_g = \sum' k_i \qquad \text{(I-7)}$$

Further, the operational form is

$$\frac{\bar{\epsilon}}{\bar{\sigma}} = k_g + \int_0^\infty \frac{L(\tau) d\tau}{\left(p + \frac{1}{\tau}\right)\tau^2} = k_g + \int_0^\infty \frac{L(\mu) d\mu}{p+\mu} \qquad \text{(I-8)}$$

c. Interrelation of the spectra. The retardation and relaxation spectra are related as indicated earlier, and the explicit relation between them will now be obtained. First note that if:

$$g(p) = \int_0^\infty f(t)\, e^{-pt}\, dt \tag{I-9}$$

$$h(s) = \int_0^\infty g(p)\, e^{-sp}\, dp \tag{I-10}$$

$$h(s) = \int_0^\infty \frac{f(t)\, dt}{s+t} \tag{I-11}$$

This iterated Laplace transform (I-11) is known as a Stieltje transform[3] and has rather simple inversion properties. Note also that, if (I-11) exists and converges, then h(s) is analytic in the entire s-plane except the negative real axis, where it has a branch point at the origin[4]. Use may be made of this cut in the principal Riemann sheet to invert (I-11):

$$h(\eta e^{-i\pi}) = \lim_{\delta\to 0} \int_0^\infty \frac{f(t)\, dt}{(t-\eta-i\delta)}, \quad \text{with } s = -\eta - i\delta,\ \eta > 0$$

$$= \lim_{\delta\to 0} \int_0^\infty \frac{f(t)(t-\eta+i\delta)\, dt}{(t-\eta)^2+\delta^2}$$

$$= \lim_{\delta\to 0} \int_0^\infty \frac{f(t)(t-\eta)\, dt}{(t-\eta)^2+\delta^2} + i \lim_{\delta\to 0} \delta \int_0^\infty \frac{f(t)\, dt}{(t-\eta)^2+\delta^2}$$

$$= \int_0^\infty \frac{f(t)\, dt}{t-\eta} + i \lim_{\delta\to 0} \delta \int_{-\pi}^{0} \frac{f(\eta+\delta\tan\theta)\,\delta\sec^2\theta\, d\theta}{\delta^2\sec^2\theta} \qquad [t-\eta = \delta\tan\theta]$$

$$= \int_0^\infty \frac{f(t)\, dt}{t-\eta} + i\pi f(\eta) \tag{I-12}$$

Similarly $$h(\eta e^{i\pi}) = \int_0^\infty \frac{f(t)\, dt}{t-\eta} - i\pi f(\eta) \tag{I-13}$$

The integrals in (12) are principal values. The difference between equations (12) and (13) is known as the jump, given by

$$h(ne^{-i\pi}) - h(ne^{i\pi}) = 2\pi i f(n) \qquad \text{(I-14)}$$

Thus, the inversion of (11) is accomplished simply by calculating the jump of the function h(s)/2πi.

Now compare equations (4) and (8) and note that

$$m_e + \int_0^\infty \frac{P}{P+\mu}\frac{H(\mu)}{\mu}\,d\mu = \frac{1}{k_g + \int_0^\infty \frac{L(\mu)\,d\mu}{P+\mu}} = m_g - \int_0^\infty \frac{H(\mu)\,d\mu}{P+\mu} \qquad \text{(I-15)}$$

Now let:

$$\delta_H = \int_0^\infty \frac{H(\mu)\,d\mu}{P+\mu} \qquad \text{(I-16)}$$

$$\delta_L = \int_0^\infty \frac{L(\mu)\,d\mu}{P+\mu}$$

This notation will be used throughout the discussion. We now have:

$$\delta_L = \frac{k_g \delta_H}{m_g - \delta_H} \qquad \text{(I-17)}$$

Application of (14) yields:

$$L(\mu) = \frac{\frac{m_g m_e}{m_g - m_e} H(\mu)}{\left[E_g - \int_0^\infty \frac{H(\xi)\,d\xi}{\xi - \mu}\right]^2 + \pi^2 [H(\mu)]^2} \qquad \text{(I-18)}$$

Later on we shall investigate various types of relaxation distribution functions and shall use (18) to determine the associated retardation spectra.

3. Distribution functions.

As indicated earlier various approximations to the shape of the distribution function can be made. Generally one is forced to compromise between complexity of the function and complexity of the resulting analysis. At this time three types of functions will be described.

a. The Power-Law Distribution Function

Before examining viscoelastic test data in detail, it is wise to investigate the general character of most creep or relaxation data. The first thing that one observes is that most materials behave in a fashion which corresponds to a straight line plot of log compliance versus log time. The log-log slope n is nearly constant. Furthermore, during relaxation, most materials display the same log-log slope, but with a negative value. Also, the real part of dynamic modulus plotted versus reciprocal frequency on log-log coordinates is strikingly similar to log relaxation modulus versus log time. Finally, creep behaves as relaxation at

reciprocal reduced time, provided unit reduced time is used to define the respective inflection points. Compliance is not reciprocal modulus, as is often incorrectly suggested, and as is shown by (18). These observations suggest a model based on a rather simple distribution function. That this indeed is the case is found by investigating the relaxation distribution function

$$H(\mu) = \frac{n\,\mu^n}{E_g}, \qquad \mu = \frac{1}{kT} \tag{I-19}$$

The reason for the proportionality constant $\frac{n}{E_g}$ will become immediately obvious.

Note that $\int_0^\infty H(\mu)\,d\ln\mu$ does not converge. Strictly speaking, in order to normalize (19), it would be necessary to assume an upper limit, say μ_m, for μ, equivalent to a lower limit, T_m, for T. In practice this lower limit is so small anyway that the neglect of the range of relaxation times shorter than T_m has no observable effect upon measured data. It is worthwhile to digress a moment to show this. In order to normalize $H(\mu)$, we write

$$H(\mu) = \begin{cases} C\mu^n, & 0 \le \mu \le \mu_m \\ 0, & \mu_m < \mu \end{cases} \tag{I-20}$$

$$1 = \int_0^\infty H(\mu)\,d\ln\mu = \int_0^{\mu_m} C\mu^{n-1}\,d\mu = C\,\frac{\mu_m^n}{n}, \quad \text{so that} \tag{I-21}$$

$$H(\mu) = \begin{cases} n\left(\frac{\mu}{\mu_m}\right)^n, & 0 \le \mu \le \mu_m \\ 0, & \mu_m < \mu \end{cases} \tag{I-22}$$

The relaxation behavior becomes in simple terms:

$$E_{rel.} = E_e + (E_g - E_e)\int_0^\infty H(\mu)e^{-\mu s}\,d\ln\mu = E_e + (E_g - E_e)\int_0^{\mu_m} n\frac{\mu^{n-1}}{\mu_m^n}e^{-\mu s}\,d\mu$$

$$= E_e + (E_g - E_e)\,\frac{n\,\gamma(n, \mu_m s)}{(\mu_m s)^n} \qquad [s = kt] \tag{I-23}$$

When the argument $\mu_m \zeta > 3$, the incomplete gamma function is excellently approximated by the complete gamma function; and since $\mu_m \zeta = \frac{t}{\tau_m}$ and since $\tau_m < 10^{-6}$ sec for most polymers at or above the transition temperature, it follows that the relaxation function becomes a straight line on log-log paper after a few microseconds (Fig. 1).

$$E_{rel.} \simeq E_e + (E_g - E_e)\frac{n\Gamma(n)}{(\mu_m \zeta)^n} = E_e + (E_g - E_e)\frac{\Gamma(1+n)}{(\mu_m \zeta)^n} \qquad (I\text{-}24)$$

$$\log\left[\frac{E_{rel.} - E_e}{E_g - E_e}\right] = \log\Gamma(1+n) - n \log \mu_m \zeta \qquad (I\text{-}25)$$

The tensile curve at constant strain rate R may be obtained by integrating (24) to:

$$\frac{\sigma_{\tau_m}}{\epsilon} = \frac{R}{\epsilon}\int_0^{\epsilon/R} E_{rel.}(\zeta)\,d\zeta = E_e + (E_g - E_e)\frac{n}{1-n}\left[\frac{\Gamma(n)}{\zeta^n} - \frac{1}{\zeta}\right] \qquad (I\text{-}26)$$

$$\zeta = \frac{\mu_m \epsilon}{R}$$

$$\simeq E_e + (E_g - E_e)\frac{\Gamma(1+n)}{(1-n)\left(\frac{\mu_m \epsilon}{R}\right)^n}, \qquad \frac{R}{\epsilon} = \text{strain rate } (\text{sec}^{-1})$$

Thus we arrive at the first simple relation deduced from the power-law with cutoff at μ_m, namely:

$$\frac{\sigma_{\tau_m}}{\epsilon} - E_e \simeq \left[\frac{E_{rel.} - E_e}{1-n}\right]_{\zeta = \frac{\epsilon}{R}}, \quad \text{or} \qquad (I\text{-}27)$$

$$\sigma_{\tau_m} = \epsilon\left[E_e + \left(\frac{E_{rel.} - E_e}{1-n}\right)_{\zeta = \frac{\epsilon}{R}}\right] \qquad (I\text{-}28)$$

Likewise, by direct calculation, it follows that:

$$\frac{E' - E_e}{E - E_e} = \frac{n}{2}\left(\frac{\Delta}{\mu_m}\right)^n B_{\frac{\mu_m^2}{\Delta^2 + \mu_m^2}}\left(\frac{n}{2}, 1 - \frac{n}{2}\right) \simeq \left(\frac{\Delta}{\mu_m}\right)^n \frac{n\frac{\pi}{2}}{\sin n\frac{\pi}{2}}, \quad \Delta = \frac{w}{R} \qquad (I\text{-}29)$$

The middle term of (29) contains the factor $B_x(p, 1\text{-}p)$ which is the incomplete Beta function, which very rapidly becomes approximated by the complete Beta function:

$$B_x(P, 1-P) \simeq B(P, 1-P) \equiv \frac{\Gamma(P)\Gamma(1-P)}{\Gamma(1)} \equiv \frac{\pi}{\sin \pi P} \qquad (I\text{-}30)$$

Based on the observation that relaxation and real part of dynamic data

are practically superimposeable, one can equate $E_{rel} = E'$:

$$\frac{\Gamma(1+n)}{(\mu_m s)^n} = \left(\frac{\omega}{\mu_m}\right)^n \frac{n\frac{\pi}{2}}{\sin n\frac{\pi}{2}} \qquad (I-31)$$

which gives

$$\omega s = \omega t = \left[\frac{2}{\pi} \sin n\frac{\pi}{2}\, \Gamma(n)\right]^{\frac{1}{n}} \qquad (I-32)$$

Note that for $n = 1$, $\omega t = \frac{2}{\pi}$ } $= .637$

$n = \frac{1}{2}$, $\omega t = \frac{2}{\pi}$ }

$n = 0$, $\omega t = e^{-\delta} = .560$

so that (cf. Fig.2), in general, ωt is well approximated by a value of 0.6.

The imaginary part of dynamic modulus is calculated to be

$$\frac{E''}{E_g - E_e} = \frac{n}{2}\left(\frac{\omega}{\mu_m}\right)^n B_{\frac{\mu_m^2}{\omega^2+\mu_m^2}}\left(\frac{1+n}{2}, \frac{1-n}{2}\right) \simeq \left(\frac{\omega}{\mu_m}\right)^n \frac{n\frac{\pi}{2}}{\cos n\frac{\pi}{2}} \qquad (I-33)$$

which leads to another simple relation:

$$\frac{E''}{E' - E_e} \simeq \tan\frac{n\pi}{2} \qquad (I-34)$$

In order to calculate the creep compliance, it is necessary to proceed via the Laplace transforms: (I-35)

$$\bar{E}_{rel.} = \frac{E_e}{p} + (E_g - E_e)\frac{n}{p}\left(\frac{p}{\mu_m}\right)^n B_{\frac{\mu_m}{p+\mu_m}}(n, 1-n) \simeq \frac{E_e}{p} + (E_g - E_e)\frac{p^{n-1}}{\mu_m^n}\frac{n\pi}{\sin n\pi}$$

$$\bar{D}_{crp.} = \frac{1}{p^2\left[\frac{E_e}{p} + (E_g - E_e)\frac{p^{n-1}}{\mu_m^n}\frac{n\pi}{\sin n\pi}\right]} \qquad (I-36)$$

At this point, it is necessary to assume $E_e \ll E_{rel}$ in order to effect the inversion; this approximation, along with the previous one of assuming $\frac{\mu_m}{p} \ll 1$ limits the application of the resulting formula to the transition region.

$$\bar{J}_{crp.} \simeq \frac{\mu_m^n \sin n\pi}{E_g\, p^{1+n}\, n\pi} \tag{I-37}$$

$$J_{crp.} \simeq \frac{(\mu_m \zeta)^n}{E_g\, \Gamma(1+n)} \frac{\sin n\pi}{n\pi} \tag{I-38}$$

This leads to another simple relation, observed between creep and relaxation:

$$J_{crp.} \cdot E_{rel.} \simeq \frac{\sin n\pi}{n\pi} \tag{I-39}$$

The complex modulus and compliance are easily obtained

$$E^* = E' + iE'' = E_e + (E_g - E_e)\frac{n\pi}{\sin n\pi} e^{in\frac{\pi}{2}} \tag{I-40}$$

$$J^* = \frac{1}{E_e + (E_g - E_e)\frac{n\pi}{\sin n\pi} e^{in\frac{\pi}{2}}} \simeq J \frac{\sin n\pi}{n\pi} e^{-in\frac{\pi}{2}} \tag{I-41}$$

It remains to connect the distributions $H(\mu)$ and $L(\mu)$. Since the exact relations involving the cutoff functions are mathematically quite involved, one can gain some insight to the relation by reverting to the function introduced in (19). We have:

$$E_{rel.} \simeq E_g \int_0^\infty \frac{H(\mu)}{\mu} e^{-\mu\zeta} d\mu = \frac{\Gamma(1+n)}{\zeta^n} \tag{I-42}$$

$$\bar{E}_{rel.} \simeq \frac{\Gamma(1+n)\,\Gamma(1-n)}{p^{1-n}} \tag{I-43}$$

$$\bar{J}_{crp.} \simeq \frac{1}{\Gamma(1+n)\,\Gamma(1-n)\,p^{1+n}} \tag{I-44}$$

$$J_{crp.} = J_e - (J_e - J_g)\int_0^\infty L(\mu)\, e^{-\mu\zeta} d\ln\mu \tag{I-45}$$

$$\bar{J}_{crp.} = \frac{J_e}{p} - (J_e - J_g)\int_0^\infty \frac{L(\mu)\, d\mu}{\mu(p+\mu)} \tag{I-46}$$

$$\bar{J}_{crp.} \simeq \frac{J_e}{p}\mathcal{L}_L \tag{I-47}$$

$$\mathcal{L}_L \simeq \frac{p}{J_e}\bar{J}_{crp.} = \frac{1}{J_e\,\Gamma(1+n)\,\Gamma(1-n)\,p^n} \tag{I-48}$$

$$L(\mu) \simeq \frac{1}{J_e\, n\, \mu^n} \tag{I-49}$$

This leads to a simple relation between the distribution functions:

$$H(\mu)\cdot L(\mu) = \frac{1}{E_g \cdot J_e} = \frac{E_e}{E_g} = \beta \qquad \text{(I-50)}$$

It is reiterated that the above relations are valid only in the transition region. Finally it is to be noted that, in this region, both distribution functions are directly proportional to the associated relaxation and creep data, at the corresponding relaxation and retardation times. Thus the creep curve traces out, as it were, the retardation spectrum. And similarly the relaxation curve traces out the relaxation spectrum.

b. The Smoothed Power Law Distribution

An alternative way of guaranteeing normalization of the power-law distribution without cutoff is by multiplying in an exponential whose argument is approximately zero in the transition region:

$$\tau D(\tau) = \frac{e^{-1/k\tau}}{\Gamma(n)(k\tau)^n} \qquad [\text{PR. \#2, P. 8}] \qquad \text{(I-51)}$$

$$H(\mu) = \frac{\mu^n e^{-\mu}}{\Gamma(n)} \qquad \int_0^\infty H(\mu)\, d\ln\mu = 1 \qquad \text{(I-52)}$$

This function (Fig. 3) is normalized to unity and has some very interesting analytical properties. The mean reciprocal relaxation time is given by

$$\langle \mu \rangle = \int_0^\infty \frac{\mu^n e^{-\mu}}{\mu}\, d\mu = n \qquad \text{(I-53)}$$

and the maximum of the curve $H(\mu)$ vs. μ occurs at n.
The relaxation function is given by:

$$E_{rel.} = E_e + (E_g - E_e)\int_0^\infty \frac{\mu^{n-1} e^{-\mu(1+\zeta)}}{\Gamma(n)}\, d\mu = E_e + \frac{E_g - E_e}{(1+\zeta)^n} \qquad \text{(I-54)}$$

and has the property that when $\zeta > 1$, it generates a straight line on log-log coordinates.

As before, tensile is obtained by integration:

$$\frac{\sigma_{tran.}}{\epsilon} = E_e + (E_g - E_e)\frac{R}{\epsilon}\,\frac{(1+\quad)^{1-n} - 1}{1-n} \qquad \text{(I-55)}$$

Application of Laplace transform to (I-54) yields

$$p\bar{E}_{rel.} = E_e + (E_g - E_e) p^n e^p \Gamma(1-n, p) \quad , \text{ so that} \tag{I-56}$$

$$\mathcal{J}_H(p) = 1 - p^n e^p \Gamma(1-n, p) \tag{I-57}$$

A complete analytical representation of (57) is given by:

$$\mathcal{J}_H(p) = 1 - e^p p^n \Gamma(1-n) + e^p p^n \sum_{m=0}^{\infty} \frac{(-1)^m p^{m+1-n}}{n!\,(m+1-n)} \tag{I-58}$$

$$= 1 - e^p p^n \Gamma(1-n) + \sum_{m=1}^{\infty} \frac{\Gamma(1-n)\, p^m}{\Gamma(m+1-n)}$$

For large p, the asymptotic expansion is: (I-59)

$$\mathcal{J}_H(p) = -\sum_{m=1}^{M-1} \frac{\Gamma(m+n)}{\Gamma(n)(-p)^m} + O\left(|p|^{-M}\right), \quad p \to \infty, \quad -\frac{3\pi}{2} < \arg p < \frac{3\pi}{2}$$

$$M = 1, 2, \cdots$$

Making use of (18), it is possible to evaluate the retardation function:

(I-60)

$$L(\mu) = \frac{\beta H(\mu)}{\left\{1 - (1-\beta)\left[1 - H(\mu)\pi \operatorname{ctn} n\pi + \sum_{m=1}^{\infty} \frac{\Gamma(1-n)(-\mu)^m}{\Gamma(m+1-n)}\right]\right\}^2 + (1-\beta)^2 \pi^2 \left[H(\mu)\right]^2}$$

or asymptotically,

(I-61)

$$L(\mu) = \frac{\beta H(\mu)}{\left\{1 - (1-\beta)\left[1 - H(\mu)\pi \operatorname{ctn} n\pi - \sum_{m=0}^{M-1} \frac{\Gamma(m+n)}{\Gamma(n)\mu^m}\right]\right\}^2 + (1-\beta)^2 \pi^2 \left[H(\mu)\right]^2}$$

Figure 4 compares the retardation and relaxation functions. The complex dynamic modulus is obtained by letting p = is in (56).

$$\frac{E' - E_e}{E_g - E_e} = \mathcal{J}^n \cos\left(\mathcal{J} + \frac{n\pi}{2}\right)\Gamma(1-n) - \sum_{m=1}^{\infty} \frac{\Gamma(1-n)(-\mathcal{J}^2)^m}{\Gamma(2m+1-n)} \tag{I-62}$$

$$\frac{E''}{E_g - E_e} = \mathcal{J}^n \sin\left(\mathcal{J} + \frac{n\pi}{2}\right)\Gamma(1-n) - \sum_{m=1}^{\infty} \frac{\Gamma(1-n)\mathcal{J}^{2m-1}(-1)^m}{\Gamma(2m-n)} \tag{I-63}$$

The associated asymptotic expansions are:

$$\frac{E' - E_e}{E_g - E_e} = \sum_{m=0}^{M-1} \frac{\Gamma(m+n)(-1)^m}{\Gamma(n)\,\Delta^{2m}} \qquad \text{(I-64)}$$

$$\frac{E''}{E_g - E_e} = \sum_{m=1}^{M-1} \frac{\Gamma(m+n)(-1)^m}{\Gamma(n)\,\Delta^{2m-1}} \qquad \text{(I-65)}$$

Figure 5 is a Nyquist diagram which shows the relation between the magnitude and phase of the complex modulus. Note that for low frequency ($s \rightarrow o$), the phase relation is given by

$$\frac{E''}{E' - E_e} = \tan\frac{n\pi}{2} \qquad \text{which is identical with (34).} \qquad \text{(I-66)}$$

Although not now available, plots of $D_{crp.}$ and D* are being prepared. The latter is obtained simply from 103, the former by (61), the algebra of which is quite involved.

c. The Cole[5] Distribution

Another distribution function, which has proved useful in fitting dynamic data (Fig.) is given by

$$H(\mu) = \frac{2\sin n\frac{\pi}{2}}{\pi\left[2\cos n\frac{\pi}{2} + \mu^n + \mu^{-n}\right]} = \frac{\sin n\frac{\pi}{2}}{\pi\left[\cos n\frac{\pi}{2} + \cosh n\ln\mu\right]} \qquad \text{(I-67)}$$

This function has the merit of casting the dynamic modulus into a rather simple form:

$$\frac{E_g - E'}{E_g - E_e} = \frac{1}{1 + s^n} \tag{I-68}$$

This relation will be used to fit experimental data on propellants. Analytic expressions for related functions such as E'', E_{rel}, G_{tens}, D_{crp} and D* are being derived.

4. Temperature-time dependence

One of the implicit assumptions made throughout the discussion, in addition to the usual ones of linearity, neglect of acceleration forces in the equilibrium equation, and small displacements, is that all relaxation and retardation times have the same temperature dependence. To understand this point, consider the general expression which represents relaxation data for any temperature in terms of a discrete model, say for simplicity in uniaxial tension where $m_i \rightarrow E_i$:

$$E_{rel} = E_e + \sum E_i e^{-t/\tau_i} \tag{I-69}$$

Now introduce the assumption

$$\tau_i = A_i f(T) \tag{I-70}$$

where A_i is independent of temperature and f(T) is independent of index "i".

$$E_{rel} = E_e + \sum E_i e^{-t/A_i f(T)} \tag{I-71}$$

The temperature dependence of the viscous component of E_{rel}, neglecting the linear dependence of the spring constants upon temperature is given by

$$\frac{\partial E_{rel}}{\partial T} = \sum E_i e^{-\frac{t}{A_i f}} \cdot \frac{t}{A_i f} \cdot \frac{f'}{f} \qquad \text{(I-72)}$$

Similarly, the temporal dependence at constant temperature is given by

$$\frac{\partial E_{rel}}{\partial \ln t} = -\sum E_i e^{-\frac{t}{A_i f}} = -\frac{f}{f'} \frac{\partial E_{rel}}{\partial T} \qquad \text{(I-73)}$$

Now write:

$$dE_{rel} = \frac{\partial E_{rel}}{\partial \ln t} d\ln t + \frac{\partial E_{rel}}{\partial T} dT$$

$$= \left(-\frac{f}{f'} d\ln t + d\xi\right) \frac{\partial E_{rel}}{\partial T} \qquad \text{(I-74)}$$

Thus, in order for dE_{rel} to be zero, which implies temperature-time equivalence, it follows that:

$$d\ln t = d\ln f(T) \quad , \quad \text{or} \qquad \text{(I-75)}$$

$$E_{rel} \equiv E_{rel}\left[t/f(T)\right] \qquad \text{(I-76)}$$

A convenient way of reducing relaxation data is to locate the geometric mean modulus at unity on the reduced time scale. When this is done, the shift factors K(t) are so defined that

$$E_{rel} = \sqrt{E_e E_g}, \text{ or } \log E_{rel} = \frac{\log E_g + \log E_e}{2} \qquad \text{(I-77)}$$

when t/K is 1, where K has the same dimension as time. Furthermore, (76) becomes

$$E_{rel} \equiv E_{rel}\left[t/K\right] \qquad \text{(I-78)}$$

and (71) becomes

$$E_{rel} = E_e + \sum E_i e^{-\frac{1}{A_i}\frac{t}{K}} \qquad \text{(I-79)}$$

It is desirable now to identify (79) with (57). This is accomplished in the following way. It has been suggested[1] that a good analytical representation for relaxation data may be obtained in terms of the error function. This suggestion stems from the fact that a plot of

$$\frac{\log E_{rel} - \log E_e}{\log E_g - \log E_e} \quad \text{vs} \quad \log \frac{t}{K} \tag{I-80}$$

gives a straight line on probability paper:

$$\log E_{rel} = \log \sqrt{E_e E_g} + \log \sqrt{\frac{E_e}{E_g}} \cdot \operatorname{erf}\left(h \log \frac{t}{K}\right) \tag{I-81}$$

where K is adjusted so that the inflection point of the relaxation curve is located at unit reduced time, and where h is the reciprocal of $\sqrt{2} \times$ standard deviation. For most polymers h is of the order of 0.4. When the argument of the error function is less than unity which implies $t/K < 300$, (81) is well approximated by

$$\log E_{rel} = \log \sqrt{E_e E_g} + \log \sqrt{\frac{E_e}{E_g}} \cdot \frac{2}{\sqrt{\pi}} h \log \frac{t}{K} \tag{I-82}$$

Thus the log-log slope is given by:

$$n = \frac{h}{\sqrt{\pi}} \log \frac{E_g}{E_e} \tag{I-83}$$

In order to adjust (54) so that the inflection point is at unity on the reduced time scale, it can be written:

$$E_{rel}-E_e=\frac{\sqrt{E_e(E_g-E_e)}}{\left[\frac{t}{K}+\left(\frac{E_e}{E_g-E_e}\right)^{\frac{1}{2n}}\right]^n} \tag{I-84}$$

which implies

$$k=\frac{1}{K}\left(\frac{E_g-E_e}{E_e}\right)^{\frac{1}{2n}}=\frac{1}{K\beta^{\frac{1}{2n}}} \tag{I-85}$$

Returning to (79), it may be rewritten (I-86)

$$E_{rel}=E_e+\sum E_i e^{-\frac{\beta^{\frac{1}{2n}}}{A_i}\xi}=E_e+\sum E_i e^{-\mu_i\xi}, \quad \text{where}$$

$$\frac{1}{\mu_i}=k\tau_i=\frac{A}{\beta^{\frac{1}{2n}}}=kKA_i, \quad \text{or} \tag{I-87}$$

$$A_i=\frac{\tau_i}{K} \tag{I-88}$$

Note that u_i is independent of temperature because A_i is by assumption and β is by definition. Thus the temperature dependence of τi is canceled by multiplication by k or division by K. By the same token, the temperature dependence of $D(\tau)$ is canceled by multiplication by τ , so that H(u) is temperature independent. Whether one chooses to reduce the time scale by K or k is purely a matter of convenience. The former factor is more easily connected with the straight line reduction of relaxation data on probability paper. The latter factor is more easily connected with the straight line reduction of relaxation data on log-log paper.

After k or K has been determined as a function of temperature, a plot usually in the form of log K vs 1/T is made and found to have a maximum at a temperature T_d, called the distinctive temperature which is usually within 10°F of the glass transition temperature. The associated value of $K = K_d$ is of the order of 2 minutes for most polymeric materials, and the product $hT_d \sim 100$. An almost universal temperature dependence of K for most polymers has been shown by Tobolsky[1] (Fig. 6) in the form

$$\log\frac{K}{K_o}=-\frac{16.14\,(T-T_o)}{56+T-T_o} \tag{I-89}$$

An alternative reduction scheme[6] casts the shift factor a_T in terms of a reference temperature T_s, which does not have the distinction of being determined independently as T_d in the Tobolsky scheme, but which was arbitrarily chosen to be -30° for unfilled polyisobutylene. From this starting point, it is possible to derive another almost universal temperature dependence for most polymers:

$$\log a_T = \frac{-8.86\,(T - T_s)}{101.8 + T - T_s} \tag{I-90}$$

Where T_s is roughly 40° higher than the glass transition temperature, and where $a_T \sim 10^3$ K/K$_d$. By the same token, the inflection point of relaxation or dynamic data will be located at 10^3 on the reduced frequency scale, or 10^{-3} on the reduced time scale. This, in effect, locates the glassy end of the modulus or compliance curve at unit reduced frequency or unit reduced time.

An important question that arises in connection with thermal stress problems may now be phrased: suppose a viscoelastic solid be subjected to a stress distribution arising from the diffusion of a thermal gradient; given that the temperature is determined at a given position and given time, what is the relaxation time below which the contribution to the viscoelastic modulus is negligible. Roughly speaking, this is equivalent to asking how many dashpots have relaxed to negligible stress at a given time and temperature.

We make use of the smoothed power law distribution and recall that:

$$\frac{E_{rel} - E_e}{E_g - E_e} = \frac{1}{(1+\xi)^n} \tag{I-91}$$

It is desired to know the highest relaxation time or lowest value of u for which the integral is negligible, say 10^{-3}:

$$\frac{E_{rel} - E_e}{E_g - E_e}\, 10^{-3} = \frac{10^{-3}}{(1+\xi)^n} = \int_{u_c}^{\infty} \frac{e^{-u} u^{n-1}\, du}{\Gamma(n)} \tag{I-92}$$

Taking n to be 0.5, it follows that

$$u_c(1+\xi) = 5.5 \quad \text{or} \quad 5.5\, k T_c = 1 + kt, \quad \text{or} \tag{I-93}$$

$$5.5\, T_c = t + \frac{1}{k} = t + h\beta \tag{I-94}$$

For all polymers

$$\beta = E_e/(E_g - E_e) \quad E_e/E_g = 10^{-3} \tag{I-95}$$

For polyurethane rubber, K_d = 2 minutes at -80°F. By (89), $K \sim 10^{-10}$ min. at +80°F, so that for all practical purposes

$$\tau_c = \frac{t}{5.5} \tag{I-96}$$

In fact, unless one is interested in very short time at very low temperatures, (96) is a useful approximation, the denominator 5.5 being determined only by the practical stress level, chosen in this case to be 10^{-3}. It is seen from (94) that the cutoff relaxation time follows the time scale of the experiment, so that, after several hours, the stress has relaxed, for all intents and purposes, to the rubbery modulus.

For filled rubbers (e.g. propellants) the above statements do not apply. Application of the WLF technique to tensile data obtained on a typical polyurethane propellant yield a standard reference temperature of $T_s = 296°K$ which is equivalent to $T_d = 0°F$, obtained by setting $T_s - T_d = 41°C$ (8). If K_d is assumed to be 2 minutes at this temperature (which is probably low for filled materials) then

at 80°F, $K = 10^{-7}$ min.

but at -60°F, $K = 10^{+21}$ min.

Thus, relaxation effects become strikingly important as the environmental temperature of the propellant is lowered. If K be interpreted as the mean relaxation time of the viscoelastic material, then one can define a temperature above which relaxation is too rapid to enter into the time scale of the problem at hand, and a temperature below which the relaxation is too slow to enter into the time scale. This follows from a straightforward application of (94) coupled with the assumption of the time scale of the experiment.

B. Response Behavior

1. Fitting distribution function to test data

The purpose of the preceding section has been to elucidate the relations which obtain among various sets of mechanical data. It was shown that the manipulation of these relations is expedited by the use of a distribution function of relaxation or retardation times. Preparatory to actually

solving engineering problems (cf. section IV), it is desirable to represent available propellant data analytically in terms of one of the afore-cited distribution functions.

Data chosen for this task are measurements of dynamic compliance of polyisobutylene filled with 37 vol. % or 60 wt. % of glass beads*; this formulation corresponds to a fairly low-filled propellant. Recently[9] other data has become available and will be used in solutions to enginerring problems. Meanwhile, the procedure will be well demonstrated with the following data.

Several attempts at rectifying the data were made. Figure 7 shows a plot on probability paper. The curve deviates markedly from linearity at either end. The standard deviation derived from this plot characterizes the propellant by h = 0.31 which is typical of many polymers[7]. Since the distribution function which corresponds to this representation has not been derived analytically, no further use will be made of it at this time.

Fig. 8 shows a log-log rectification which should correspond to the smoothed power law distribution. Failure to adequately represent the data is shown by the marked deviation of the curve from the straight line in the rubbery region.

An excellent rectification is obtained from a plot (Fig. 9) of

$$\log\left(\frac{D_e - D'}{D' - D_g}\right) \quad \text{vs} \quad \log(\omega a_T) \tag{I-97}$$

leading to the representation

$$\frac{D' - D_g}{D_e - D_g} = \frac{1}{1 + (0.0316\,\omega a_T)^{0.605}} = \frac{1}{1 + \lambda^n} \tag{I-98}$$

with $k = \frac{1}{.0316 a_T}$, as defined relative to 12.5°C by (90) with T_s = -23°C. Inversion of (98) leads to the Cole distribution (67), which is completely specified by the parameter n = .605.

---

*The values of a_T incorporated in the abscissa variables of Figures differ from those calculated by (90) by the factor ~ 200.

2. Dynamic behavior of models

In the first two progress reports operational moduli and compliances were presented for various models which implicitly related stress to strain. In addition, time dependent solutions were given for certain simple loading conditions such as the variation of strain with time when a constant load was applied. This was called a creep test, and the ratio of strain $\epsilon(t)$ to stress σ_o was defined as the creep compliance k(t).

In the fourth report, it was pointed out that a convenient method of determining model parameters involved the use of complex (or dynamic) moduli and compliances that relate sinusoidal time-dependent stress and strain. Therefore, for convenience, a table of these moduli and compliances corresponding to several models will be presented. They are obtained by formally substituting $i\omega$ (ω = frequency, $i = \sqrt{-1}$) for the time derivative symbol $P = \frac{d}{dt}$ in the operator equations given in table I.[11] The symbols will be similar to those used previously in the general presentation in that m^* will denote complex modulus while k^* denotes complex compliance. When these are used in a specific example, it will be necessary to indicate whether they represent simple tension, bulk, or shear behavior. This is done by using the symbols in table I.[11] For example, the complex shear compliance is denoted by $J^*(\omega)$, and the complex shear modulus by $G^*(\omega)$.

For simplicity, complex notation is used, e.g. sinusoidal stress is written as $\sigma_o e^{i\omega t}$ and sinusoidal strain as $\epsilon_o e^{i\omega t}$. If stress is given, σ_o is considered to be a real constant representing the maximum amplitude of the sine wave, and ϵ_o is a complex function of frequency ω. For $\sigma_o = 1$, ϵ_o is identically the dynamic compliance k^*. Similarly, with strain given, ϵ_o is real and σ_o is a complex function of frequency which is identical with the dynamic or complex modulus when $\epsilon_o = 1$. It is convenient to represent the modulus by its real and imaginary components $m'(\omega)$ and $m''(\omega)$:

$$m^*(\omega) = m'(\omega) + i\,m''(\omega) = \frac{\sigma}{\epsilon} = \frac{\sigma_o e^{i\omega t}}{\epsilon_o e^{i\omega t}} = \frac{\sigma_o}{\epsilon_o} \qquad \text{(I-99)}$$

and the compliance by its real and imaginary components $k'(\omega)$ and $-k''(\omega)$:

$$k^*(\omega) = k'(\omega) - i\,k''(\omega) = \frac{\epsilon}{\sigma} = \frac{\epsilon_o}{\sigma_o}\frac{e^{i\omega t}}{e^{i\omega t}} = \frac{\epsilon_o}{\sigma_o} \qquad \text{(I-100)}$$

Due to viscosity, there is a phase angle between stress and strain which is

$$\delta = \tan^{-1}\frac{m''(\omega)}{m'(\omega)} = \tan^{-1}\frac{k''(\omega)}{k'(\omega)} \qquad \text{(I-101)}$$

The strain lags behind the stress so that $m'(\omega), m''(\omega), k'(\omega), k''(\omega)$ are all positive functions of frequency. The complex quantities in (I-99) and (I-100) may be written in the following form

$$m^*(\omega) = |m^*| e^{i\delta}$$
$$k^*(\omega) = |k^*| e^{-i\delta} \tag{I-102}$$

where

$$|m^*| = \sqrt{(m')^2 + (m'')^2}$$
$$|k^*| = \sqrt{(k')^2 + (k'')^2}$$

Since

$$m^*(\omega) = \frac{\sigma}{\epsilon} = \frac{1}{k^*} \quad \text{or} \quad m^*(\omega)\, k^*(\omega) = 1 \tag{I-103}$$

it follows that

$$|m^*|\,|k^*| = 1 \tag{I-104}$$

which is useful in converting data from compliances to moduli or vice versa.

In order to clarify the procedure in determining the complex moduli and compliances from operational expressions, consider as an example the Voigt model. From table I the operational modulus is

$$m(p) = m_v(\tau_v p + 1) \tag{I-105}$$

Letting $p \to i\omega$

$$m^*(\omega) = m_v + i\omega m_v \tau_v \tag{I-106}$$

which gives m' and m'' as

$$m' = m_v$$
$$m'' = m_v \tau_v \omega$$

The operational compliance is

$$k(p) = \frac{1}{m(p)} = \frac{1}{m_v(\tau_v p + 1)} = \frac{k_v}{(\tau_v p + 1)} \tag{I-107}$$

Letting $p \to i\omega$

$$k^*(\omega) = \frac{k_v(1 - i\omega\tau_v)}{(1 + \omega^2 \tau_v^2)} \tag{I-108}$$

so that

$$k' = \frac{k_v}{(1 + \omega^2 \tau_v^2)}$$

$$k'' = \frac{\omega \tau_v k_v}{(1 + \omega^2 \tau_v^2)}$$

where we have defined $k_\nu = \frac{1}{m_\nu}$

Complex moduli and compliances for several models are given in Figs. I-10 through I-15. It was mentioned[11] previously that when model response is to be related to test data it is most convenient to use models consisting of Voigt elements in series if stress is given; while if strain is given, models consisting of Maxwell elements in parallel should be used. Similarly, it is desirable to represent the dynamic behavior of Voigt type models by complex compliances and dynamic behavior of Maxwell type models by complex moduli. Except in the case of the basic two-element models, this rule is followed in presenting the dynamic moduli and compliances. The notation corresponds to that proposed by the Committee on Nomenclature of the Society of Rheology[14].

3. Fitting finite-element models to test data

a. Spectral analysis of load: A brief discussion was given in the previous progress report on a method suggested by Lee[15] by which finite-element models can be determined so as to approximate actual propellant response. The method involves the use of complex frequency dependent moduli or compliances in fitting models to experimental data. The response of a finite-element model, in general, can be made to correspond approximately to actual behavior only over a narrow frequency band; thus, it is first necessary to determine the range of interest by making a Fourier analysis of the loading function. In order to evaluate this approach, the specific example of a pressurized case-bonded grain will be considered. However, at this point only the pressure has to be defined; the geometry will not enter in until after model parameters are calculated.

A pressure pulse is transient rather than periodic so that it cannot be represented exactly by a series of discrete frequency components; but rather, it must be given by a Fourier integral in which frequency is a continuous variable. Nevertheless, for practical purposes, it is sufficient to consider the grain to be loaded by periodic pulses spaced far enough apart that most of the strain introduced by one pulse relaxes out before the next one is applied. Clearly, then, the response to each of the widely separated pulses is very nearly the same as for the transient load. Consequently the important frequencies in a transient pulse can be determined if we consider not only the time scale of interest in regard to the

possibility of mechanical failure, but also the viscous properties of the propellant.

For our example, it will be assumed that pressure $P_i(t)$ increases linearly with time from $P_i = 0$ to $P_i = P_o$ at $t = t_1$, and then remains constant. In addition we will assume that from the standpoint of failure, response only up to $t = 3t_1$ need be considered. Thus, the periodic function shown in Fig. I-16 will be used in the analysis. Symmetrical waves are indicated since they lead to a simpler series than obtained if the pressure is removed instantaneously. The number of terms required to represent the function sufficiently well by a finite Fourier series will now be found. As a criterion of accuracy, we have chosen the ratio of root mean square error between the series $S_m(t)$ and the exact function $P_i(t)$ to the pressure averaged over its time of application. This is indicated by α_m in the figure. α_m can be calculated quite readily as a function of t_1/T_F and m by the relation[16]:

$$\frac{1}{T}\int_0^T \left[P_i(t) - S_m(t)\right]^2 dt = \frac{1}{T}\int_0^T P_i^2(t)\,dt - \frac{1}{2}\sum_{n=1,3,\cdots}^{m} a_n^2 \qquad \text{(I-109)}$$

where a_n are the Fourier coefficients in the cosine series

$$S_m(t) = \sum_{n=1,3,\cdots}^{m} a_n \cos\frac{2n\pi t}{T_F}$$

where

$$a_n = \frac{4P_o T_F}{\pi^2 t_1}\frac{1}{n^2}\sin\frac{n\pi t_1}{T_F}\sin\frac{3n\pi t_1}{T_F}$$

From symmetry (I-109) can be written as

$$\frac{4}{T_F}\int_0^{\frac{T_F}{4}} \left[P_i(t) - S_m(t)\right]^2 dt = \frac{4}{T_F}\int_0^{\frac{T_F}{4}} P_i^2(t)\,dt - \frac{1}{2}\sum_{n=1,3\cdots}^{m} a_n^2 \qquad \text{(I-110)}$$

yielding for α_m

$$\alpha_m^2 = \frac{256}{27}\left(\frac{t_1}{T_F}\right)\left[1 - \frac{3}{2\pi^4}\left(\frac{T_F}{t_1}\right)^3 \sum_{n=1,3,\cdots}^{m}\frac{1}{n^4}\sin^2\frac{n\pi t_1}{T_F}\sin^2\frac{3n\pi t_1}{T_F}\right] \qquad \text{(I-111)}$$

which is plotted in Fig. I-16.

We now choose the value of t_1/T_F such that the time between the end of one pulse and the start of the next is twice the total length of a single pulse $(4t_1)$. Subsequently, when the solution to the strain analysis problem is obtained a check must be made to see if the time between pulses $(8t_1)$ is sufficient for most of the strain to relax out. Thus, we take

$$\frac{T_F}{2} = 4t_1 + 8t_1 = 12t_1$$

or

$$\frac{t_1}{T_F} = \frac{1}{24}$$

In addition, we assume that when $\alpha_m \leq 0.05$ the function is given accurately enough by a finite series terminating with $n = m$. From Fig. I-16 we take $m = 13$. The lowest frequency (f) in the series is

$$f = \frac{1}{T_p}$$

and the highest

$$f = \frac{13}{T_p}$$

In terms of t_1

$$\frac{1}{24 t_1} \leq f \leq \frac{13}{24 t_1}$$

A typical value of 0.01 seconds will be used for t_1, so that

$$4 \text{ CPS} \leq f \leq 52 \text{ CPS} \qquad \text{(I-112)}$$

b. Graphical determination of model parameters: In view of the present lack of appropriate data on propellants, the analysis will be carried out using the dynamic shear data in Fig. I-17, which was obtained by Landel[17] and is for NBS polyisobutylene (PIB) filled with 36.7% (vol.) glass beads. This idealized filled material exhibits the same qualitative behavior as a typical composite propellant, so that the results should be very useful in evaluating the model fitting technique when applied to propellants.

In practice one is given a temperature and then the shift factor a_T is found (see previous section under Model Theory); however for our analysis it is desirable to choose a_T in the example such that PIB responds to pressure with a significant time effect. It was found that the value $a_T \doteq 52$ gives the desired result if $t_1 = 0.01$ seconds. It should be noted that the plot in Fig I-17 is for 12.5°C which is not the standard reference temperature ($T_s = -23$°C) for PIB with 36.7% filler. Therefore the temperature shift factor shown in the abscissa is denoted as a'_T and is defined to be unity at 12.5°C. The value of a_T we have chosen for the example corresponds to $a'_T = 10^4$. This corresponds to -35°F for PIB (with a highly filled propellant the time effect is quite significant at temperatures on the order of +40°F due to the compactness of the filler).

The frequency shift, being exponential in temperature, is much more important than the linear shift in the ordinate indicated in reference (17); so for simplicity we will consider only the effect of temperature on the frequency scale given by a'_T. This allows us to use the master curve drawn at 12.5°C directly for any temperature since

$$LOG_{10}\omega = LOG_{10}\omega a_T' - LOG_{10}a_T' = LOG_{10}\omega a_T' - 4 \qquad \text{(I-113)}$$

That is, by subtracting four from the abscissa values, the actual compliance frequency curve is obtained for use in the example. Since frequency on the master curve is in terms of radians, it will be convenient to express the frequency range given in equation (I-112) in terms of $\omega = 2\pi f$:

$$1.4 \leq LOG_{10}\omega \leq 2.5$$

or

$$5.4 \leq LOG_{10}\omega a_T' \leq 6.5 \qquad \text{(I-114)}$$

Now that the frequency range of interest and temperature are specified the model parameters can be determined using a method described by Bland and Lee[18]. It is shown in their paper that a simple graphical scheme may be used if the model contains no more than four elements; i.e. two dashpots and two springs. Therefore we will use the four-element model in Fig. I-12a and, as special cases, the two-element Voigt and Maxwell models in Fig. I-10a. It should be remarked that the models generally can be chosen independently of whether the material is crosslinked or non-crosslinked. It will be recalled that a non-crosslinked polymer strains indefinitely under a constant load; and that, in principle, this should be accounted for by a free dashpot such as in Fig. I-10b. However, when the frequency band does not include $\omega = 0$ such behavior does not appear. In addition, if the material is enclosed in a case under constant internal pressure, unlimited flow is prohibited due to the presence of a bulk modulus which causes the strain to approach a definite limiting value.

The complex compliance of the four-element model is obtained from Fig. I-12a ; however shear behavior is to be represented by the model so we let $k \to J$ and write the real and imaginary components as

$$J'(\omega) = J_g + \frac{J_1}{\omega^2\tau_1^2 + 1} \qquad \text{(I-115a)}$$

$$J''(\omega) = \frac{1}{\omega\eta} + \frac{\omega\tau_1 J_1}{\omega^2\tau_1^2 + 1} \qquad \text{(I-115b)}$$

In order to make a strain analysis of a case-bonded grain it is usually necessary to know two different moduli or compliances. Thus, in addition to the complex shear compliance, the bulk modulus K will be used. A reasonable assumption is that bulk response is elastic so that K is constant. A typical value for K is 2×10^6 psi or 13.8×10^{10} dynes/cm^2. With this in mind it will be convenient to consider the nondimensional compliance KJ^*. Defining

$$\Phi'(\omega) = KJ'(\omega) \quad , \quad \Phi''(\omega) = KJ''(\omega)$$
$$\beta_3 = KJ_3 \quad , \quad \beta_1 = KJ_1 \quad , \quad \beta_2 = \frac{K\tau_1}{\eta} \tag{I-116}$$

the compliances (I-115a) and (I-115b) become

$$\Phi'(\omega) = \beta_3 + \frac{\beta_1}{\omega^2\tau_1^2+1} \tag{I-117a}$$

$$\Phi''(\omega) = \frac{\beta_2}{\omega\tau_1} + \frac{\beta_1\omega\tau_1}{\omega^2\tau_1^2+1} \tag{I-117b}$$

Φ' and Φ'' can be combined to yield

$$\omega\Phi''(\omega) = -\frac{1}{\tau_1}\Phi'(\omega) + \frac{\beta_1+\beta_2+\beta_3}{\tau_1} \tag{I-118}$$

which is the equation of a straight line if $\omega\Phi''(\omega)$ is plotted against $\Phi'(\omega)$. The slope is $-\frac{1}{\tau_1}$ and the intercept on the $\omega\Phi''(\omega)$ axis is $\frac{\beta_1+\beta_2+\beta_3}{\tau_1}$. Hence, by plotting the experimental data of Fig. I-17 using $\omega\Phi''$ and Φ' as coordinates, the model parameters τ_1 and $\beta_1+\beta_2+\beta_3$ are determined by a best straight line fit in the previously estimated frequency band. This is done in Fig. I-18, and the parameters are found graphically to be

$$\beta_1+\beta_2+\beta_3 = 66$$
$$\tau_1 = 0.925 \times 10^{-2} \text{ SEC.}$$

Now that τ_1 is known, it can be used to plot experimental values of Φ' against $(\omega^2\tau_1^2+1)^{-1}$. It is seen from equation (I-117a) that the four-element model is again represented by a straight line, but now with slope β_1 and with β_3 as the Φ' intercept. Carrying this out we find from Fig. I-19 that

$$\beta_1 = 50 \quad , \quad \beta_3 = 6.5$$

and

$$\beta_2 = 9.5$$

The parameters in the two-element models of Fig. I-10 will now be determined. In terms of shear behavior, the complex compliance for the Voigt model is given by

$$J'(\omega) = \frac{J_v}{\omega^2\tau_v^2+1} \tag{I-119a}$$

$$J''(\omega) = \frac{\omega\tau_v J_v}{\omega^2\tau_v^2+1} \tag{I-119b}$$

Defining

$$\Phi'(\omega) = K J'(\omega) \quad , \quad \Phi''(\omega) = K J''(\omega) \quad , \quad \beta_v = K J_v \qquad \text{(I-120)}$$

the nondimensional compliances for the Voigt model are

$$\Phi'(\omega) = \frac{\beta_v}{\omega^2 \tau_v^2 + 1} \qquad \text{(I-121a)}$$

$$\Phi''(\omega) = \frac{\omega \tau_v \beta_v}{\omega^2 \tau_v^2 + 1} \qquad \text{(I-121b)}$$

These are the same as Φ' and Φ'' for the four-element model if we set $\beta_2 = \beta_g = 0$, $\beta_v = \beta_1$, and $\tau_v = \tau_1$. Thus, the straight line equation (I-118) reduces to

$$\omega \Phi''(\omega) = -\frac{1}{\tau_v} \Phi'(\omega) + \frac{\beta_v}{\tau_v} \qquad \text{(I-122)}$$

β_v and τ_v are given immediately from Fig. I-18, as

$$\beta_v = 66 \quad , \quad \tau_v = 0.925 \times 10^{-2} \text{ SEC.}$$

Fig. I-10b provides us with the complex compliance of the Maxwell model

$$\Phi'(\omega) = \beta_m \qquad \text{(I-123a)}$$

$$\Phi''(\omega) = \frac{1}{\omega \beta} \qquad \text{(I-123b)}$$

where

$$\Phi'(\omega) = K J'(\omega) \quad , \quad \Phi''(\omega) = K J''(\omega) \quad , \quad \beta_m = K J_m \quad , \quad \frac{1}{\beta} = \frac{K J_m}{\tau_m} \qquad \text{(I-124)}$$

β_m and β are determined numerically such that Φ' and Φ'' take on the experimental values approximately half-way between the frequency limits, indicated in Fig. I-18 as

$$\beta_m = 30 \quad , \quad \beta = \frac{1}{3200} = 0.312 \times 10^{-3} \text{ SEC.}$$

The four-element model can be reduced immediately to the three-element model in Fig. I-11a by setting $\eta = \infty$, and by definition this requires that $\beta_2 = 0$ in equations (I-117) and (I-118). It is observed that with three elements

$$\beta_1 + \beta_g = 66$$

and further, from (I-117) that when $(\omega^2 \tau_1^2 + 1) = 1$,

$$\beta_1 + \beta_g = 66 = \Phi'$$

Reference to Fig. I-19 shows that a straight line passing through $\Phi' = 66$ at $(\omega^2 \tau_1^2 + 1) = 1$ fits the experimental curve best if the Φ' intercept is zero. This requires $\beta_g = 0$, thereby reducing the model to the Voigt.

Thus, four elements must be used to obtain a better fit than offered by two which justifies omission of the three-element model in the strain analysis problem.

The nondimensional compliances Φ' and Φ'' are plotted in Fig. I-20 for all three models and compared with the experimental data. In addition, the compliances for the four-element model are shown in Fig. I-17 in order to clearly illustrate how the model response compares with the entire experimental master curves. It is interesting to note that both Φ' and Φ'' for four elements are reasonably close to the actual response. However, with the Maxwell model Φ' is in considerable error, while Φ'' is somewhat better. Conversely, with the Voigt model Φ' is satisfactory while Φ'' deviates considerably from the experimental values.

In the Engineering Analysis section all three models will be used in the strain analysis of a case-bonded grain, and their respective responses will be compared.

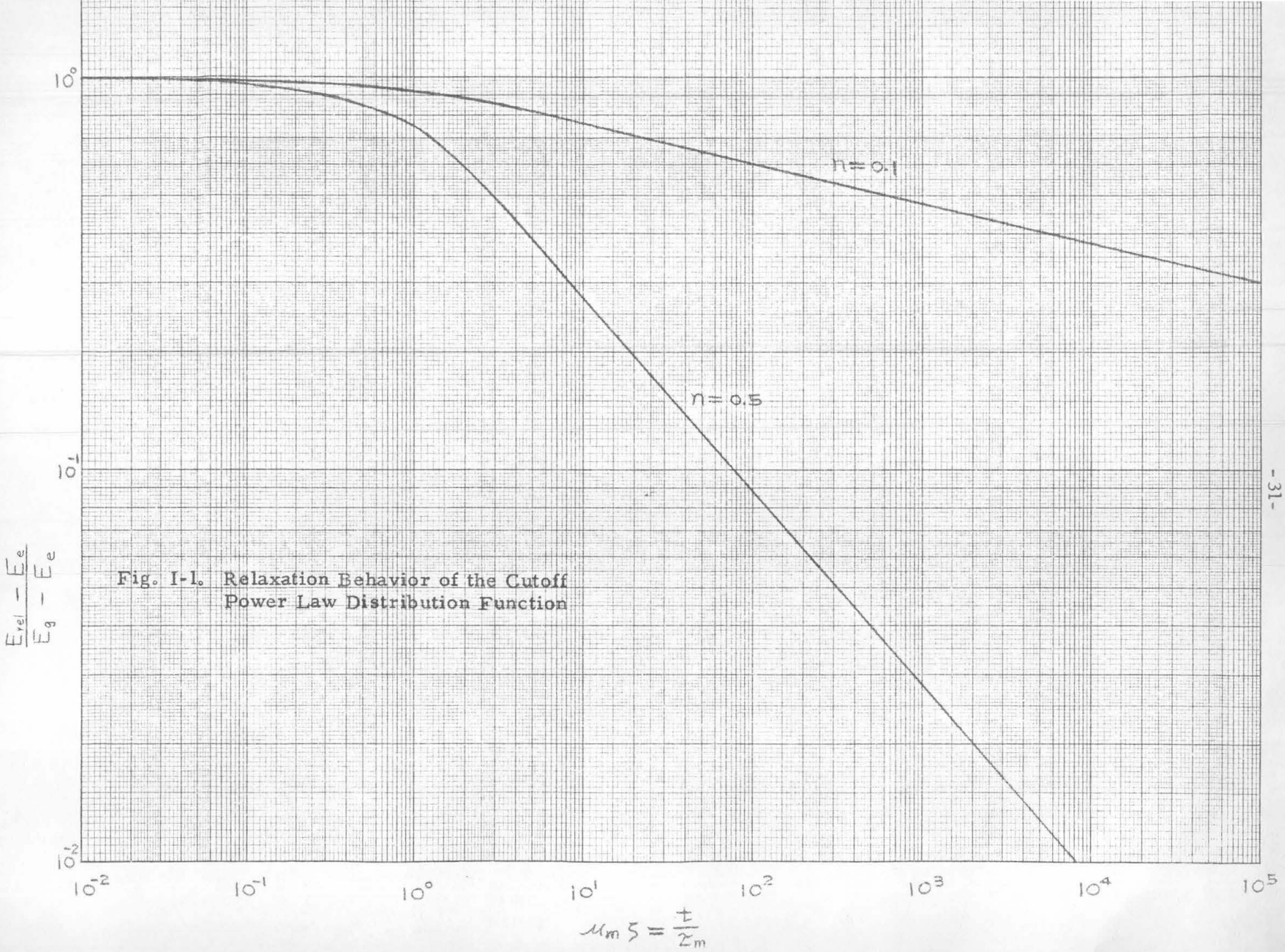

Fig. I-1. Relaxation Behavior of the Cutoff Power Law Distribution Function

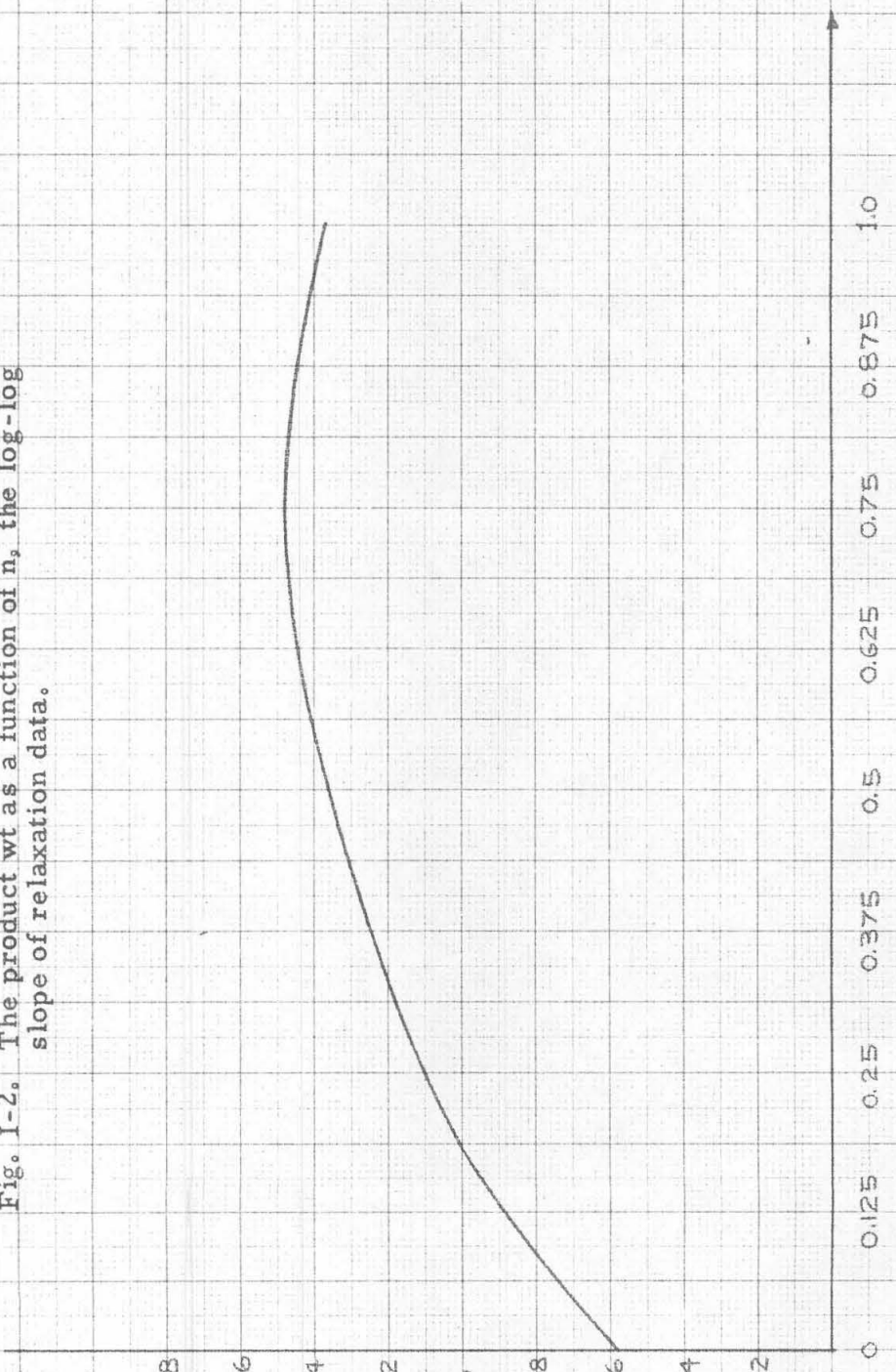

Fig. I-2. The product wt as a function of n_s the log-log slope of relaxation data.

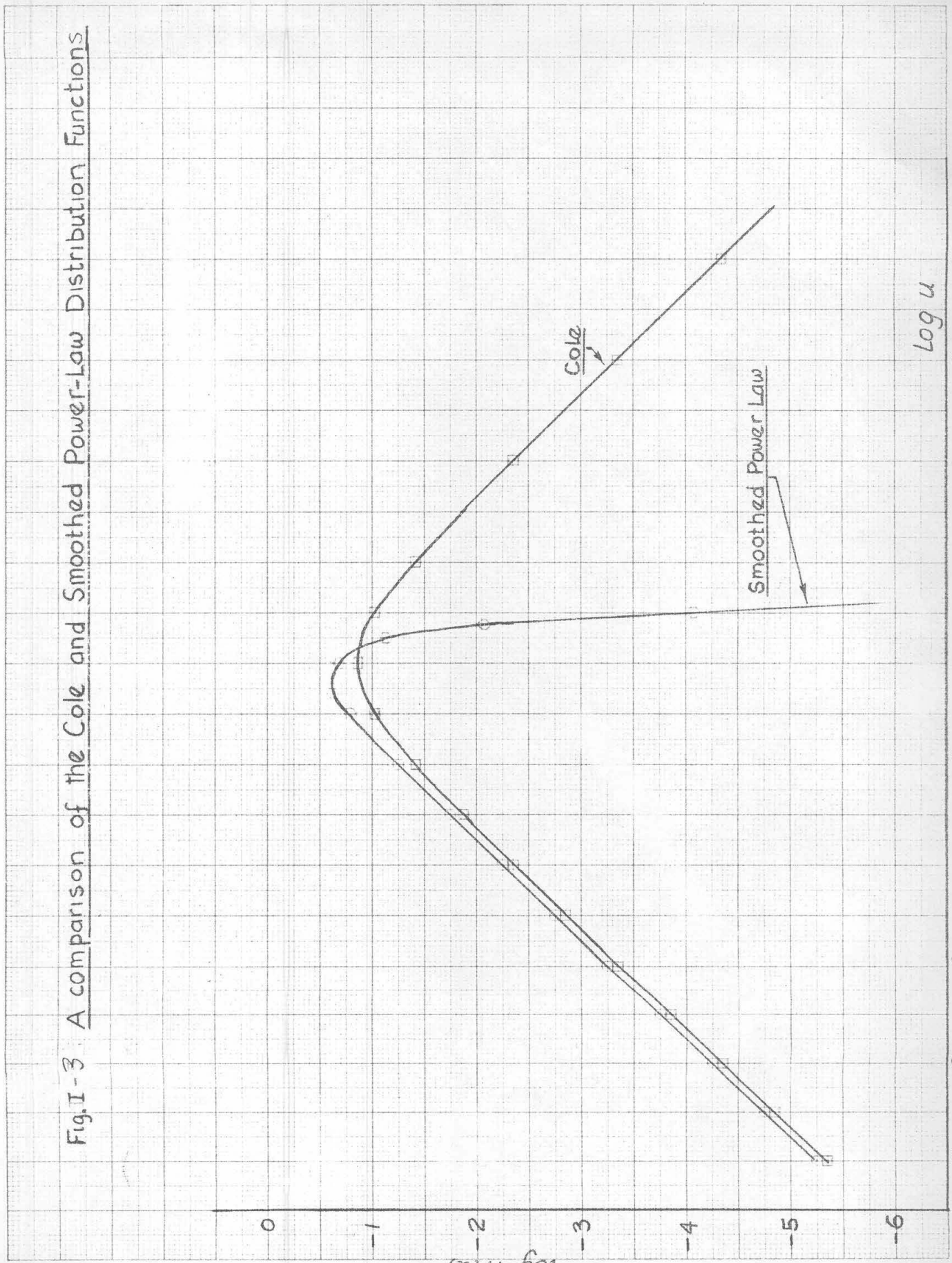

Fig. I-3 A comparison of the Cole and Smoothed Power-Law Distribution Functions

Fig. I-4. A comparison of the Smoothed Power Law relaxation spectrum and its associated retardation spectrum for $n = 0.5$

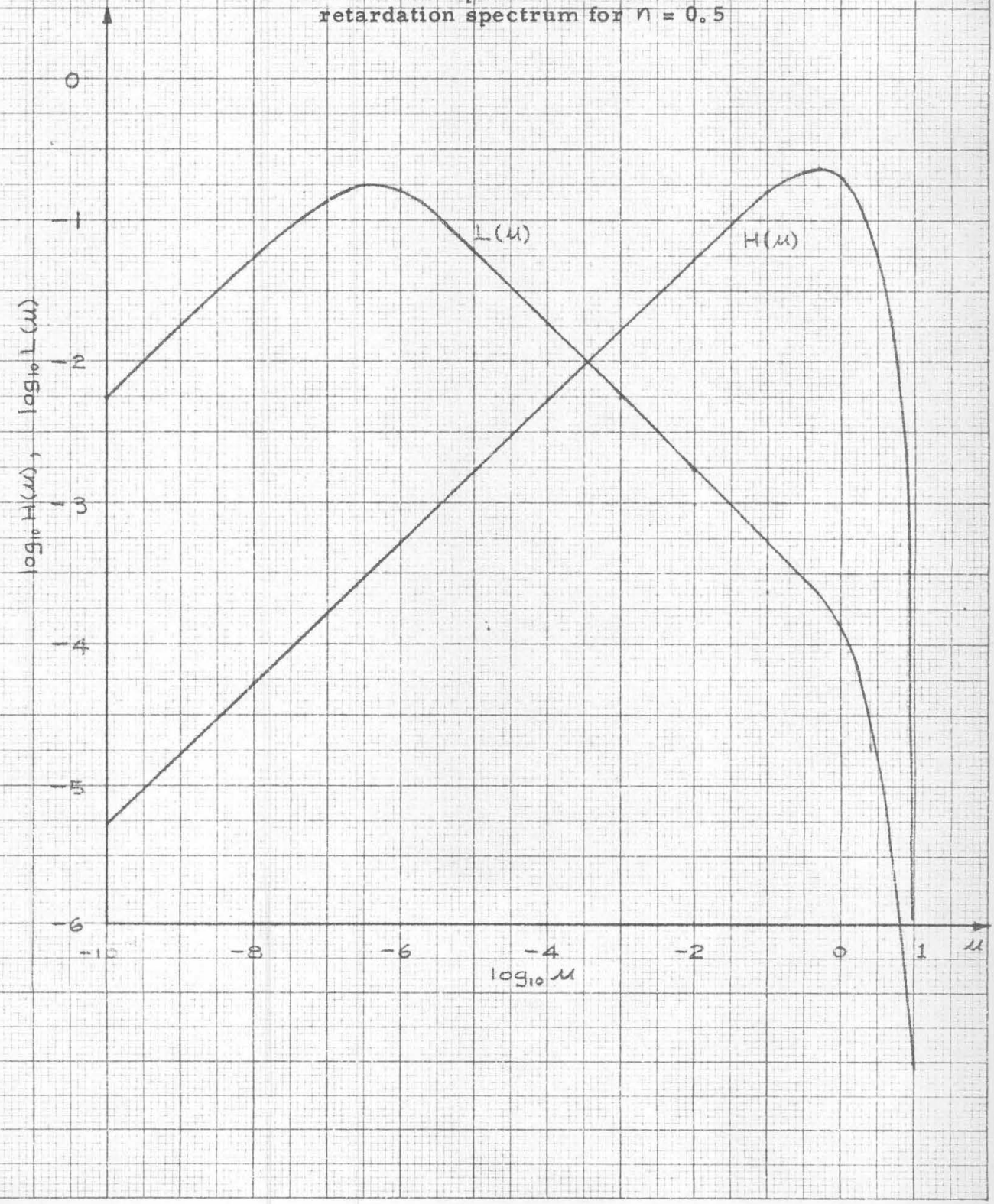

Fig. I-5. Nyquist Diagram of the Smoothed Power Law Transfer Function for $n = .12$

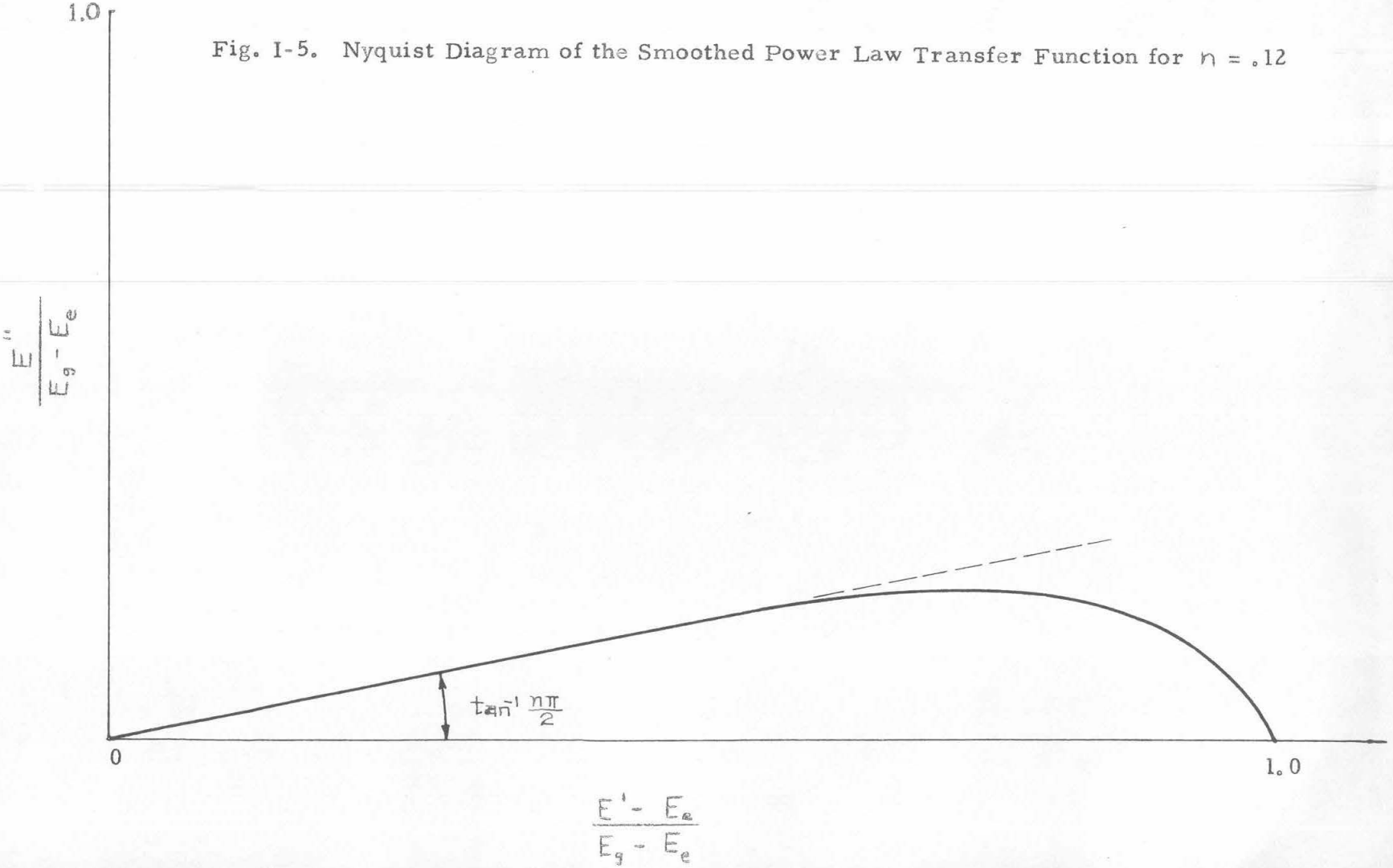

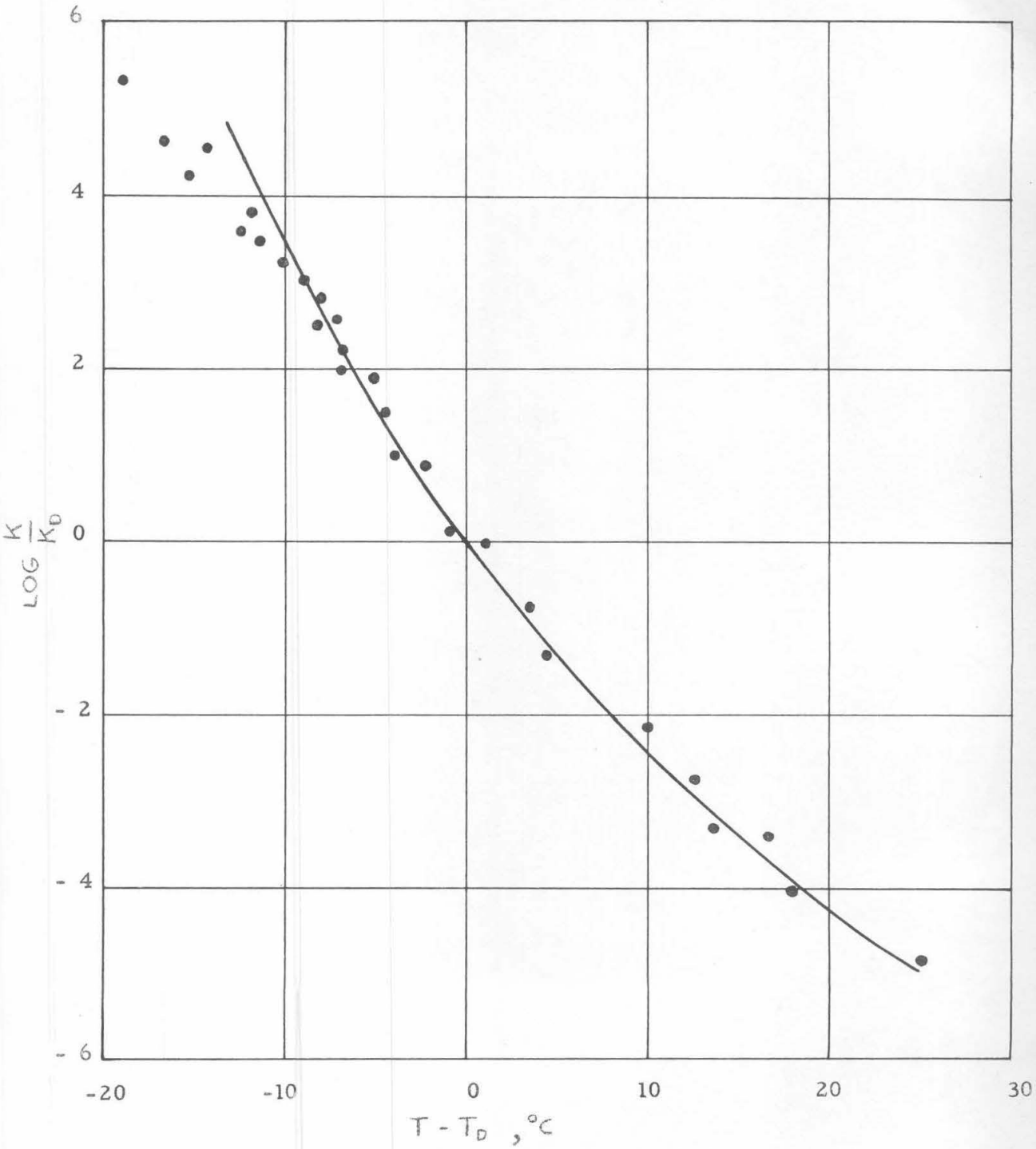

Fig. I-6. Tobolsky Curve for Reduced Shift Factors

Fig. I-7 Rectification of Dynamic Compliance Data in terms of Error Function.

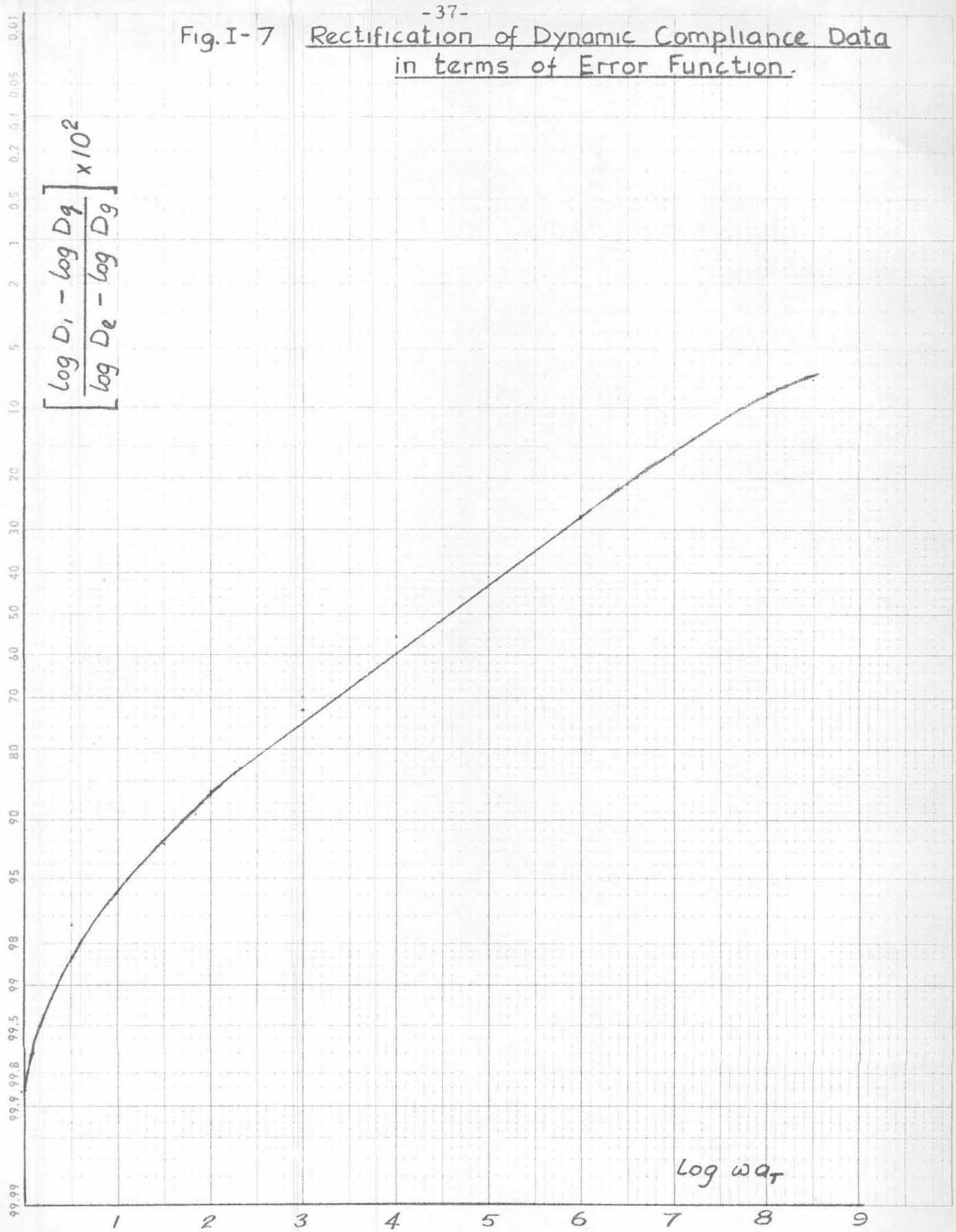

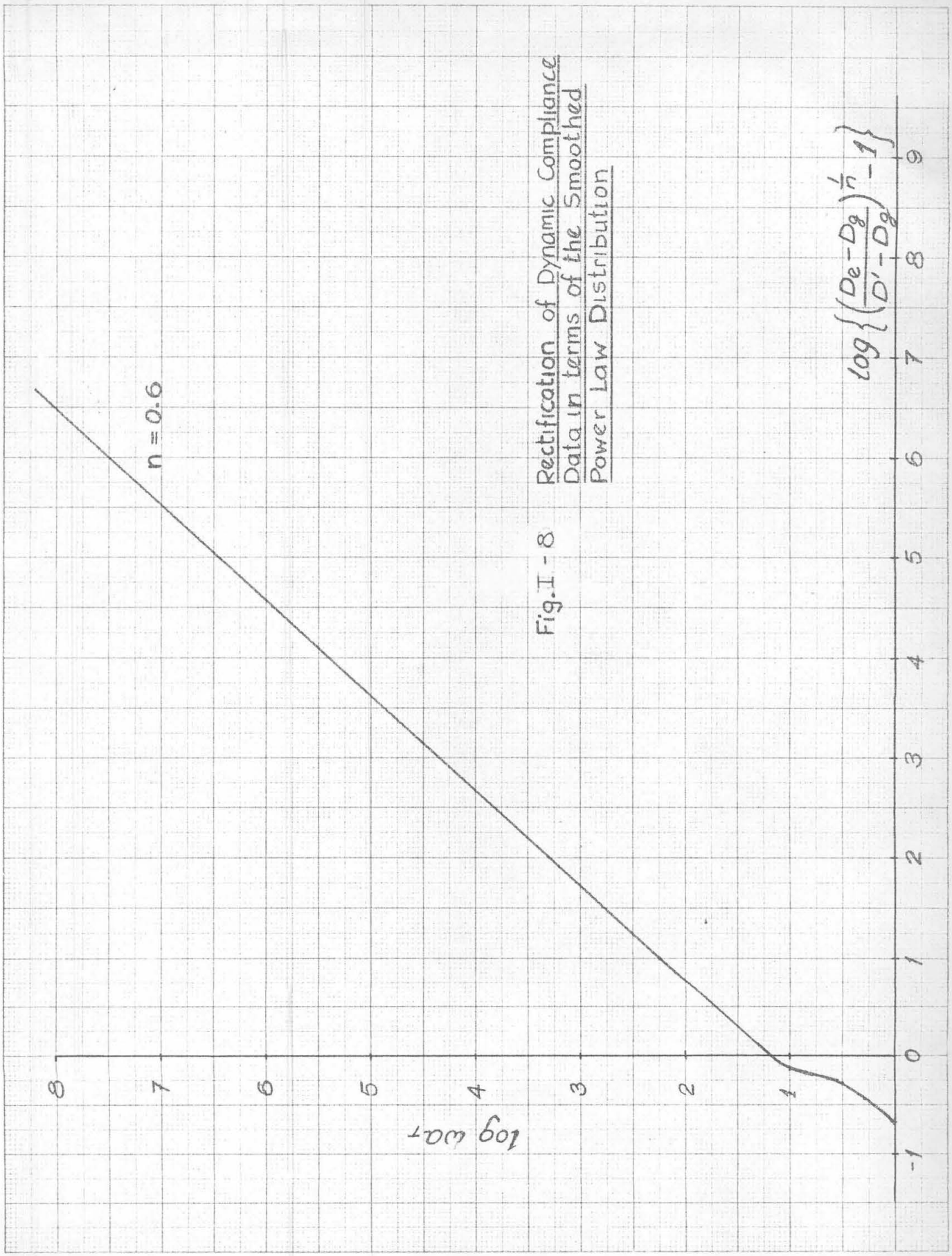

Fig. I - 8 Rectification of Dynamic Compliance Data in terms of the Smoothed Power Law Distribution

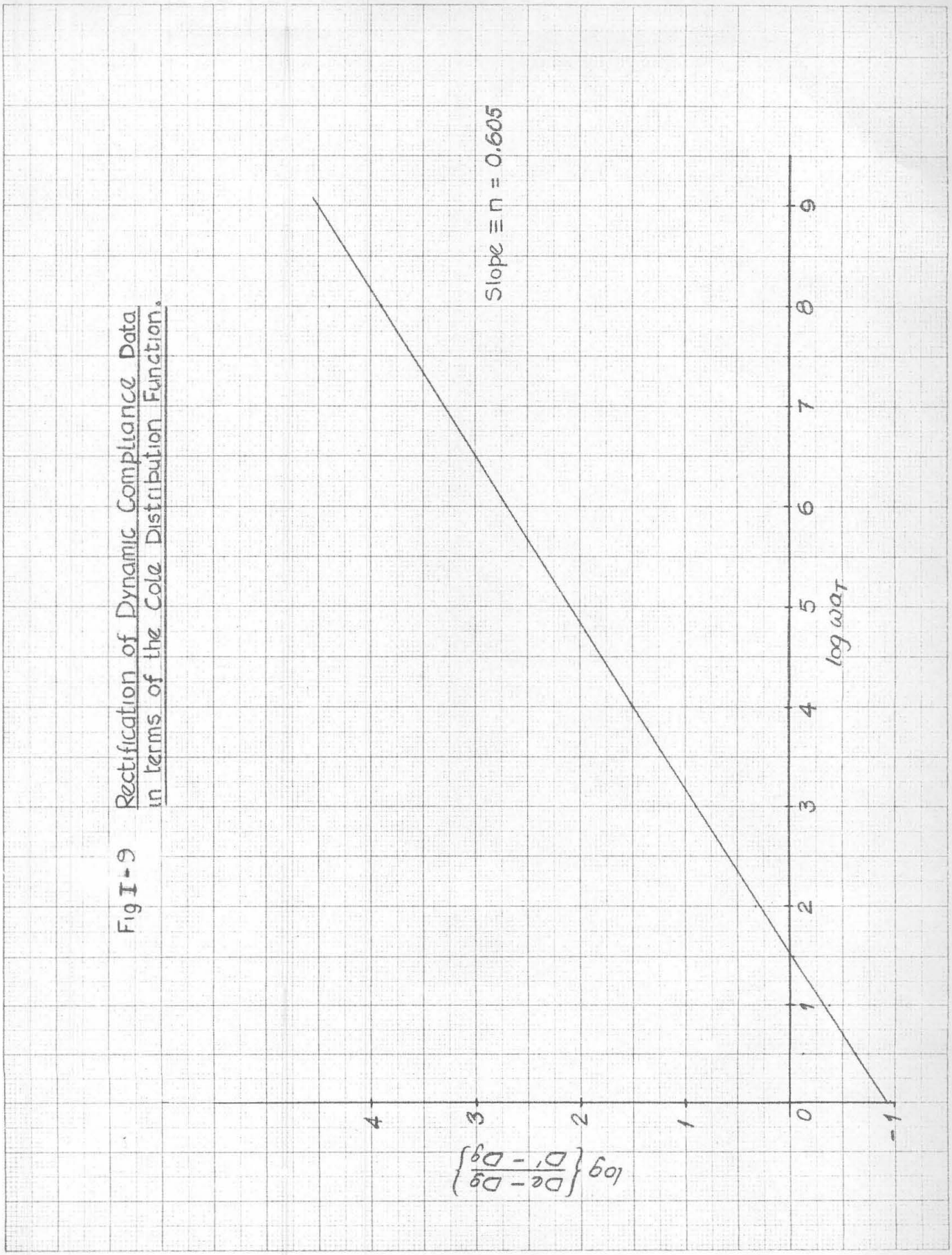

Fig I-9 Rectification of Dynamic Compliance Data in terms of the Cole Distribution Function.

OPERATIONAL COMPLIANCE: $k(p) = \dfrac{k_v}{\tau_v p + 1}$

COMPLEX COMPLIANCE: $k^*(\omega) = k'(\omega) - i\,k''(\omega)$

$$k'(\omega) = \frac{k_v}{\omega^2 \tau_v^2 + 1}$$

$$k''(\omega) = \frac{\omega \tau_v k_v}{\omega^2 \tau_v^2 + 1}$$

OPERATIONAL MODULUS: $m(p) = m_v(\tau_v p + 1)$

COMPLEX MODULUS: $m^*(\omega) = m' + i\,m''(\omega)$

$$m' = m_v$$

$$m''(\omega) = m_v \tau_v \omega$$

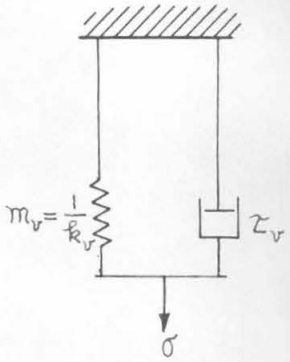

(a) VOIGT MODEL

OPERATIONAL COMPLIANCE: $k(p) = k_m + \dfrac{k_m}{\tau_m p}$

COMPLEX COMPLIANCE: $k^*(\omega) = k'(\omega) - i\,k''(\omega)$

$$k' = k_m$$

$$k''(\omega) = \frac{k_m}{\omega \tau_m}$$

OPERATIONAL MODULUS: $m(p) = \dfrac{m_m \tau_m p}{\tau_m p + 1}$

COMPLEX MODULUS: $m^*(\omega) = m'(\omega) + i\,m''(\omega)$

$$m'(\omega) = \frac{\omega^2 \tau_m^2 m_m}{\omega^2 \tau_m^2 + 1}$$

$$m''(\omega) = \frac{\omega \tau_m m_m}{\omega^2 \tau_m^2 + 1}$$

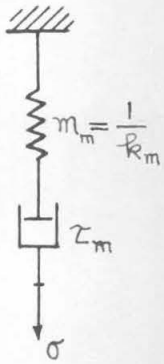

(b) MAXWELL MODEL

FIG. I-10. DYNAMIC BEHAVIOR OF TWO-ELEMENT MODELS

OPERATIONAL COMPLIANCE: $k(p) = k_g + \frac{k_1}{\tau_1 p + 1}$

COMPLEX COMPLIANCE: $k^*(\omega) = k'(\omega) - i k''(\omega)$

$$k'(\omega) = k_g + \frac{k_1}{\omega^2 \tau_1^2 + 1}$$

$$k''(\omega) = \frac{\omega \tau_1 k_1}{\omega^2 \tau_1^2 + 1}$$

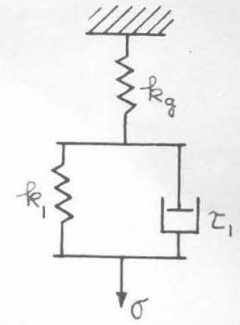

(a) VOIGT ELEMENT IN SERIES WITH GLASSY SPRING

OPERATIONAL MODULUS: $m(p) = m_e + \frac{m_1 \tau_1 p}{\tau_1 p + 1}$

COMPLEX MODULUS: $m^*(\omega) = m'(\omega) + i m''(\omega)$

$$m'(\omega) = m_e + \frac{\omega^2 \tau_1^2 m_1}{\omega^2 \tau_1^2 + 1}$$

$$m''(\omega) = \frac{\omega \tau_1 m_1}{\omega^2 \tau_1^2 + 1}$$

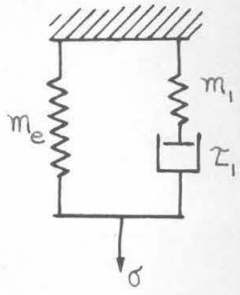

(b) MAXWELL ELEMENT IN PARALLEL WITH EQUILIBRIUM (RUBBERY) SPRING

FIG. I-11. DYNAMIC BEHAVIOR OF EQUIVALENT THREE-ELEMENT MODELS

OPERATIONAL COMPLIANCE: $k(p) = k_g + \frac{1}{\eta p} + \frac{k_1}{\tau_1 p + 1}$

COMPLEX COMPLIANCE: $k^*(\omega) = k'(\omega) - i\,k''(\omega)$

$$k'(\omega) = k_g + \frac{k_1}{\omega^2 \tau_1^2 + 1}$$

$$k''(\omega) = \frac{1}{\omega \eta} + \frac{\omega \tau_1 k_1}{\omega^2 \tau_1^2 + 1}$$

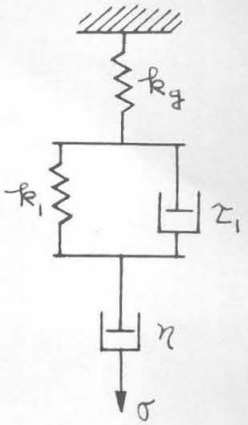

(a) VOIGT ELEMENT IN SERIES WITH MAXWELL ELEMENT

OPERATIONAL MODULUS: $m(p) = \frac{m_1 \tau_1 p}{\tau_1 p + 1} + \frac{m_2 \tau_2 p}{\tau_2 p + 1}$

COMPLEX MODULUS: $m^*(\omega) = m'(\omega) + i\,m''(\omega)$

$$m'(\omega) = \frac{\omega^2 \tau_1^2 m_1}{\omega^2 \tau_1^2 + 1} + \frac{\omega^2 \tau_2^2 m_2}{\omega^2 \tau_2^2 + 1}$$

$$m''(\omega) = \frac{\omega \tau_1 m_1}{\omega^2 \tau_1^2 + 1} + \frac{\omega \tau_2 m_2}{\omega^2 \tau_2^2 + 1}$$

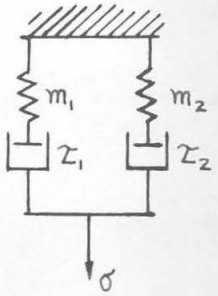

(b) TWO MAXWELL ELEMENTS IN PARALLEL

FIG. I-12 DYNAMIC BEHAVIOR OF EQUIVALENT FOUR-ELEMENT MODELS

OPERATIONAL COMPLIANCE : $k(p) = k_g + \frac{k_1}{\tau_1 p + 1} + \frac{k_2}{\tau_2 p + 1}$

COMPLEX COMPLIANCE : $k^*(\omega) = k'(\omega) - i\, k''(\omega)$

$$k'(\omega) = k_g + \frac{k_1}{\omega^2 \tau_1^2 + 1} + \frac{k_2}{\omega^2 \tau_2^2 + 1}$$

$$k''(\omega) = \frac{\omega \tau_1 k_1}{\omega^2 \tau_1^2 + 1} + \frac{\omega \tau_2 k_2}{\omega^2 \tau_2^2 + 1}$$

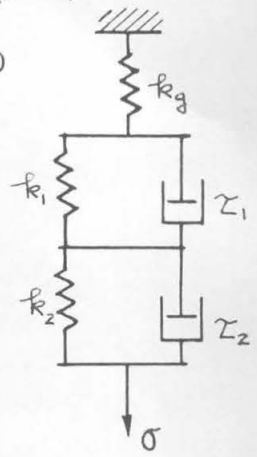

(a) TWO VOIGT ELEMENTS IN SERIES WITH GLASSY SPRING

OPERATIONAL MODULUS : $m(p) = m_e + \frac{m_1 \tau_1 p}{\tau_1 p + 1} + \frac{m_2 \tau_2 p}{\tau_2 p + 1}$

COMPLEX MODULUS : $m^*(\omega) = m'(\omega) + i\, m''(\omega)$

$$m'(\omega) = m_e + \frac{\omega^2 \tau_1^2 m_1}{\omega^2 \tau_1^2 + 1} + \frac{\omega^2 \tau_2^2 m_2}{\omega^2 \tau_2^2 + 1}$$

$$m''(\omega) = \frac{\omega \tau_1 m_1}{\omega^2 \tau_1^2 + 1} + \frac{\omega \tau_2 m_2}{\omega^2 \tau_2^2 + 1}$$

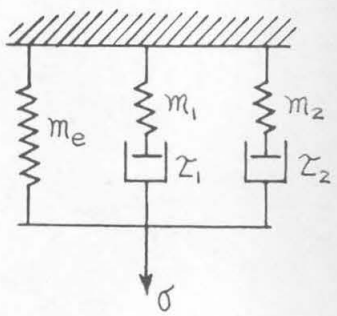

(b) TWO MAXWELL ELEMENTS IN PARALLEL WITH EQUILIBRIUM SPRING

FIG. I-13. DYNAMIC BEHAVIOR OF EQUIVALENT FIVE-ELEMENT MODELS

OPERATIONAL COMPLIANCE: Finite n; $k(p) = k_g + \sum_{i=1}^{n} \frac{k_i}{\tau_i p + 1}$

$$n = \infty; \qquad k(p) = k_g + \int_0^\infty \frac{L(\tau)}{(\tau p + 1)} \frac{d\tau}{\tau}$$

COMPLEX COMPLIANCE: $k^*(\omega) = k'(\omega) - i\,k''(\omega)$

Finite n; $k'(\omega) = k_g + \sum_{i=1}^{n} \frac{k_i}{\omega^2 \tau_i^2 + 1}$, $k''(\omega) = \sum_{i=1}^{n} \frac{\omega \tau_i k_i}{\omega^2 \tau_i^2 + 1}$

$$n = \infty; \qquad k'(\omega) = k_g + \int_0^\infty \frac{L(\tau)\, d\tau}{(\omega^2 \tau^2 + 1)\tau}, \quad k''(\omega) = \int_0^\infty \frac{\omega \tau L(\tau)}{(\omega^2 \tau^2 + 1)} \frac{d\tau}{\tau}$$

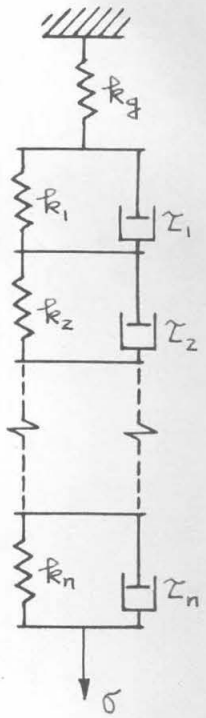

(a) n VOIGT ELEMENTS IN SERIES WITH GLASSY SPRING (KELVIN)

OPERATIONAL MODULUS: Finite n; $m(p) = m_e + \sum_{i=1}^{n} \frac{m_i \tau_i p}{\tau_i p + 1}$

$$n = \infty; \qquad m(p) = m_e + \int_0^\infty \frac{H(\tau)\tau p}{(\tau p + 1)} \frac{d\tau}{\tau}$$

COMPLEX MODULUS: $m^*(\omega) = m'(\omega) + i m''(\omega)$

Finite n; $m'(\omega) = m_e + \sum_{i=1}^{n} \frac{\omega^2 \tau_i^2 m_i}{\omega^2 \tau_i^2 + 1}$

$$m''(\omega) = \sum_{i=1}^{n} \frac{\omega \tau_i m_i}{\omega^2 \tau_i^2 + 1}$$

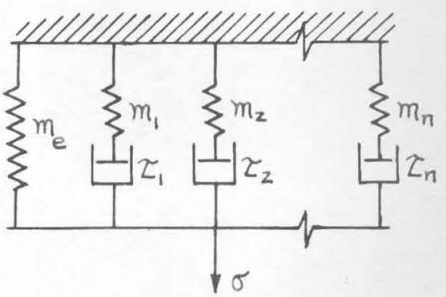

$$n = \infty; \quad m'(\omega) = m_e + \int_0^\infty \frac{\omega^2 \tau^2 H(\tau)}{(\omega^2 \tau^2 + 1)} \frac{d\tau}{\tau}; \qquad m''(\omega) = \int_0^\infty \frac{\omega \tau H(\tau)}{(\omega^2 \tau^2 + 1)} \frac{d\tau}{\tau}$$

(b) n MAXWELL ELEMENTS IN PARALLEL WITH EQUILIBRIUM SPRING (WIECHERT)

FIG. I-14 DYNAMIC BEHAVIOR OF EQUIVALENT KELVIN AND WIECHERT MODELS

OPERATIONAL COMPLIANCE: Finite n ; $k(p) = k_g + \frac{1}{\eta p} + \sum_{i=1}^{n} \frac{k_i}{\tau_i p + 1}$

$$n = \infty ; \qquad k(p) = k_g + \frac{1}{\eta p} + \int_0^\infty \frac{L(\tau)}{(\tau p + 1)} \frac{d\tau}{\tau}$$

COMPLEX COMPLIANCE: $k^*(\omega) = k'(\omega) - i\, k''(\omega)$

Finite n ; $\qquad k'(\omega) = k_g + \sum_{i=1}^{n} \frac{k_i}{\omega^2 \tau_i^2 + 1}$

$$k''(\omega) = \frac{1}{\eta \omega} + \sum_{i=1}^{n} \frac{\omega \tau_i k_i}{\omega^2 \tau_i^2 + 1}$$

$n = \infty$; $\qquad k'(\omega) = k_g + \int_0^\infty \frac{L(\tau)}{(\omega^2 \tau^2 + 1)} \frac{d\tau}{\tau}$

$$k''(\omega) = \frac{1}{\eta \omega} + \int_0^\infty \frac{\omega \tau L(\tau)}{(\omega^2 \tau^2 + 1)} \frac{d\tau}{\tau}$$

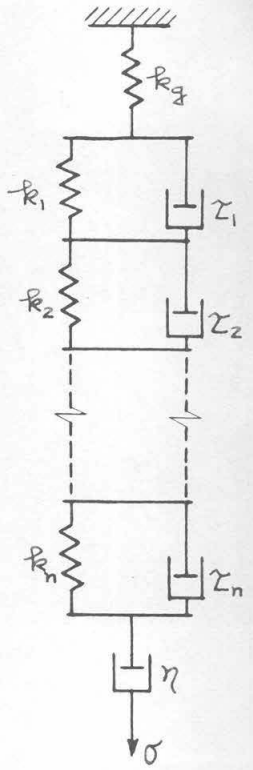

(a) n VOIGT ELEMENTS IN SERIES WITH MAXWELL ELEMENT (KELVIN)

OPERATIONAL MODULUS: Finite n ; $m(p) = \sum_{i=1}^{n+1} \frac{m_i \tau_i p}{\tau_i p + 1}$

$$n = \infty ; \qquad m(p) = \int_0^\infty \frac{H(\tau) \tau p}{(\tau p + 1)} \frac{d\tau}{\tau}$$

COMPLEX MODULUS: $m^*(\omega) = m'(\omega) + i\, m''(\omega)$

Finite n ; $\qquad m'(\omega) = \sum_{i=1}^{n+1} \frac{\omega^2 \tau_i^2 m_i}{\omega^2 \tau_i^2 + 1}$

$$m''(\omega) = \sum_{i=1}^{n+1} \frac{\omega \tau_i m_i}{\omega^2 \tau_i^2 + 1}$$

$n = \infty$; $\quad m'(\omega) = \int_0^\infty \frac{\omega^2 \tau^2 H(\tau)}{(\omega^2 \tau^2 + 1)} \frac{d\tau}{\tau}$; $\qquad m''(\omega) = \int_0^\infty \frac{\omega \tau H(\tau)}{(\omega^2 \tau^2 + 1)} \frac{d\tau}{\tau}$

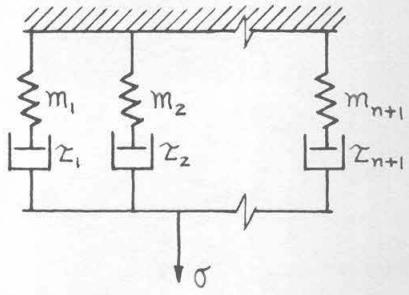

(b) (n+1) MAXWELL ELEMENTS IN PARALLEL (WIECHERT)

FIG. I-15 DYNAMIC BEHAVIOR OF EQUIVALENT KELVIN AND WIECHERT MODELS

FIG. I-16 RATIO OF ROOT MEAN SQUARE ERROR TO AVERAGE VALUE OF PRESSURE PULSE FOR FINITE FOURIER SERIES APPROXIMATION

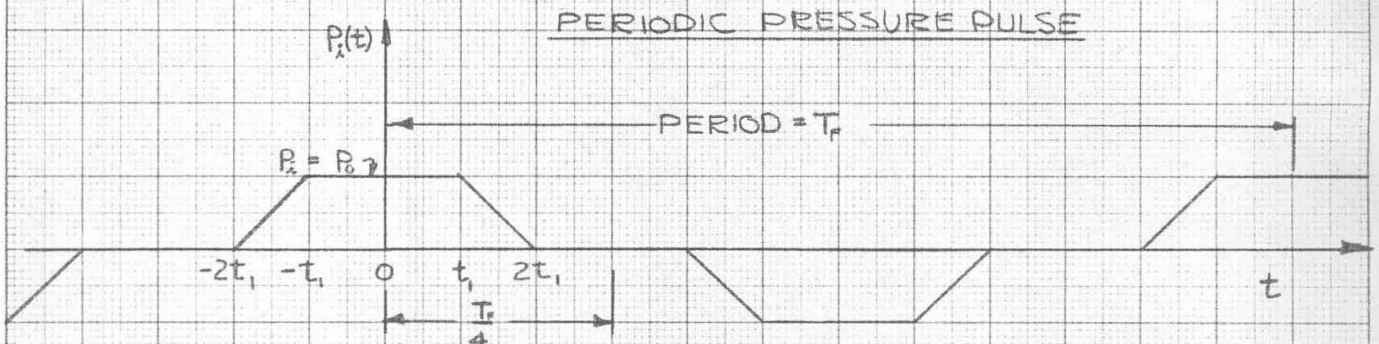

$$\alpha_m = \frac{\left\{\frac{4}{T_F}\int_0^{\frac{T_F}{4}}\left[P_i(t) - S_m(t)\right]^2 dt\right\}^{\frac{1}{2}}}{\frac{1}{2t_1}\int_0^{2t_1} P_i(t)\,dt}$$

WHERE

$$S_m(t) = \frac{4P_0}{\pi^2}\frac{T_F}{t_1}\sum_{n=1,3,5\cdots}^{m}\frac{1}{n^2}\sin\frac{n\pi t_1}{T_F}\sin\frac{3n\pi t_1}{T_F}\cos\frac{2n\pi t}{T_F}$$

$S_m(t) \rightarrow P_i(t)$ AS $m \rightarrow \infty$

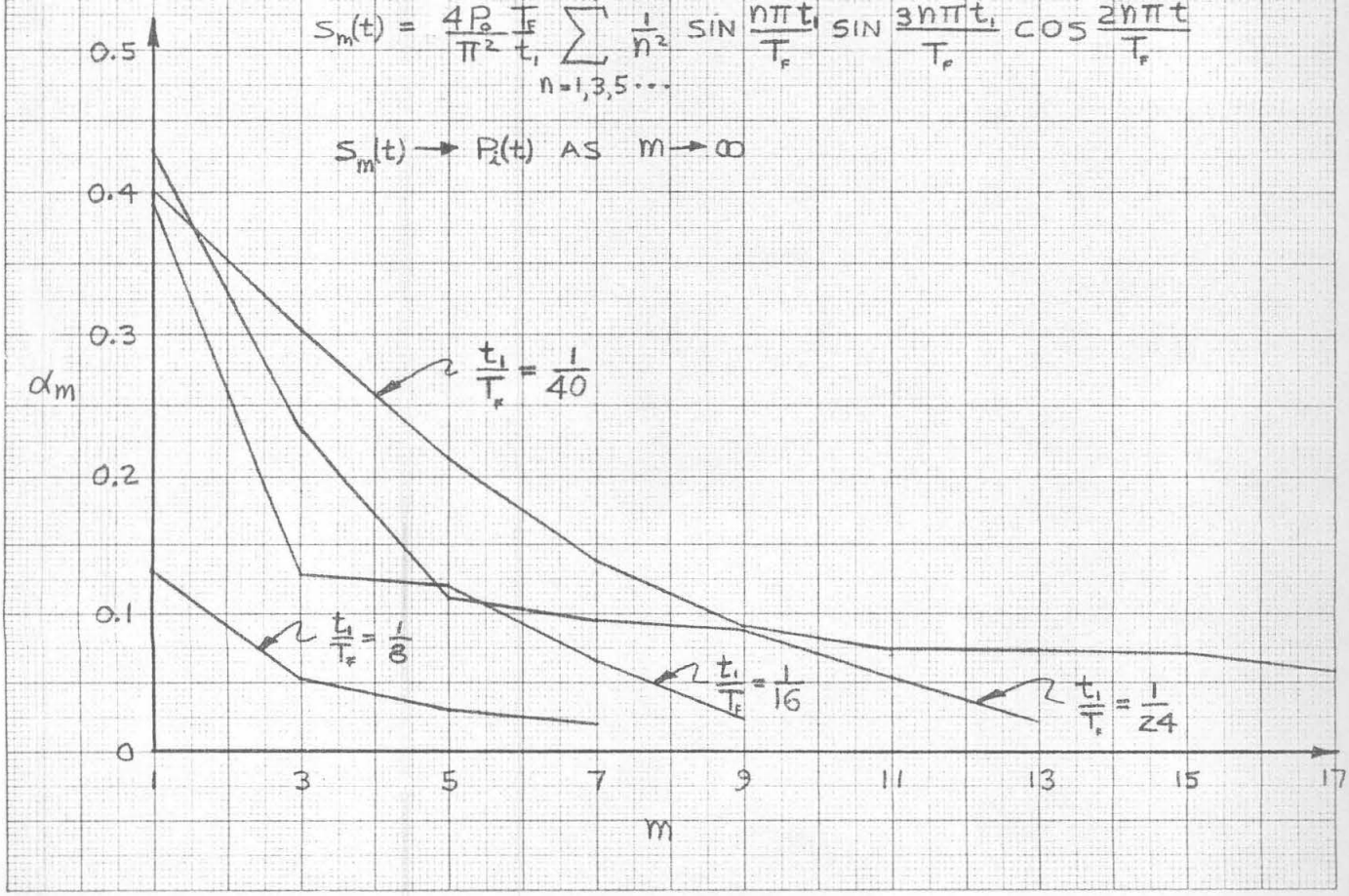

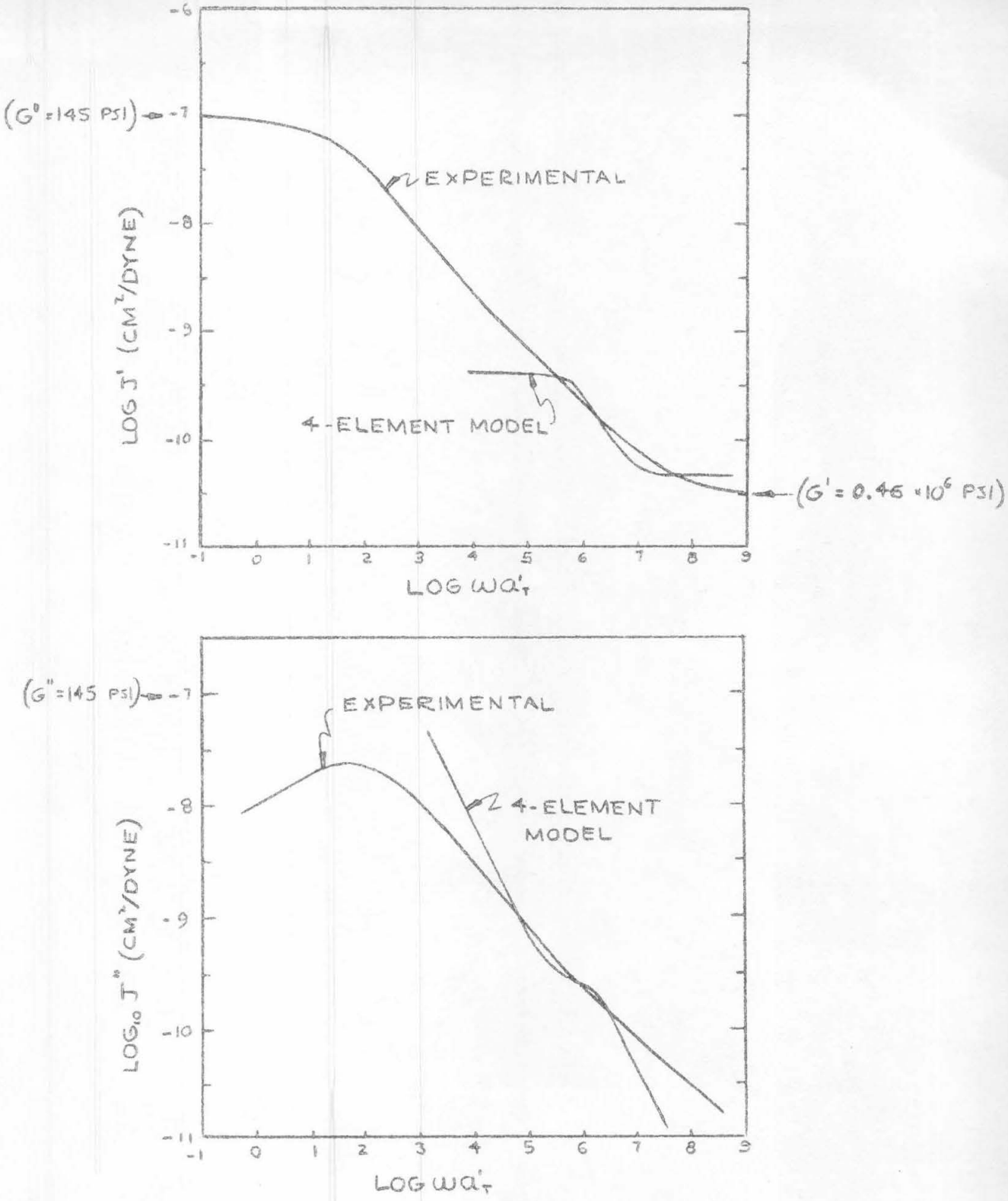

FIG I-17 MASTER CURVES FOR REAL AND IMAGINARY COMPONENTS OF COMPLEX COMPLIANCE AT 54.5°F (12.5°C) (NBS POLYISOBUTYLENE)

FIG. I-18 PLOT FOR DETERMINING 2 AND 4-ELEMENT MODEL PARAMETERS (FOR PIB AT -35°F)

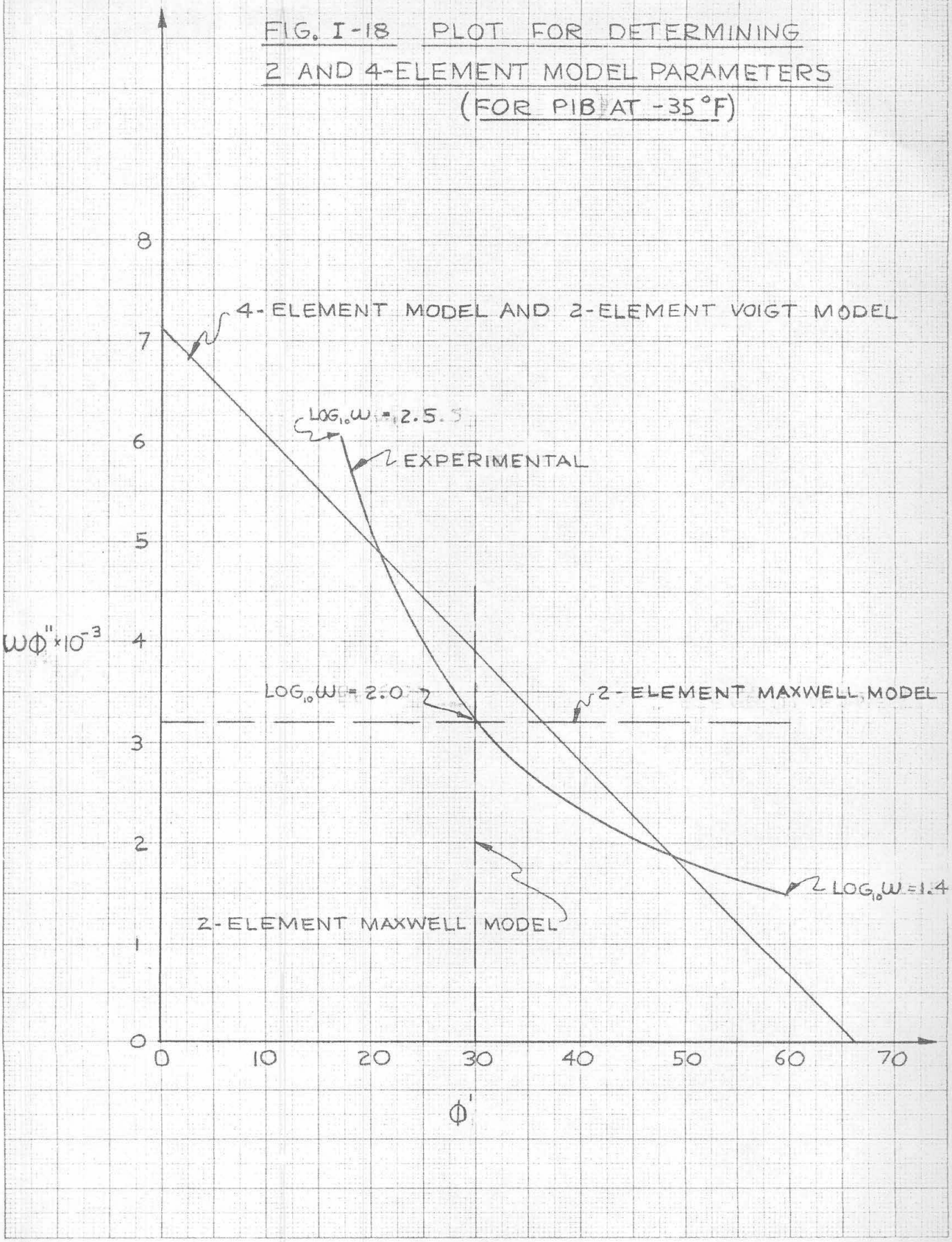

FIG. I-19 PLOT FOR DETERMINING 4-ELEMENT MODEL PARAMETERS (FOR PIB AT -35°F)

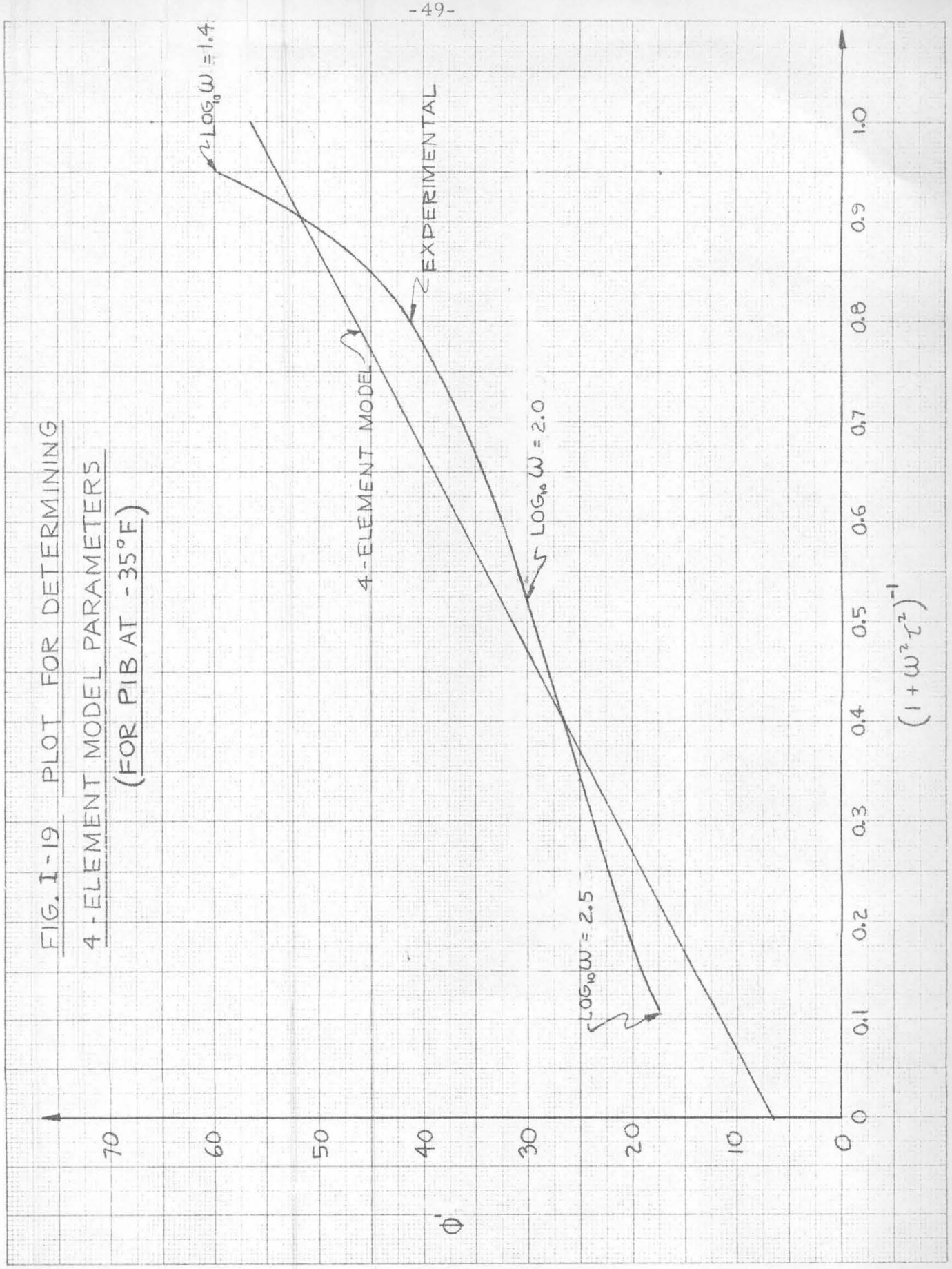

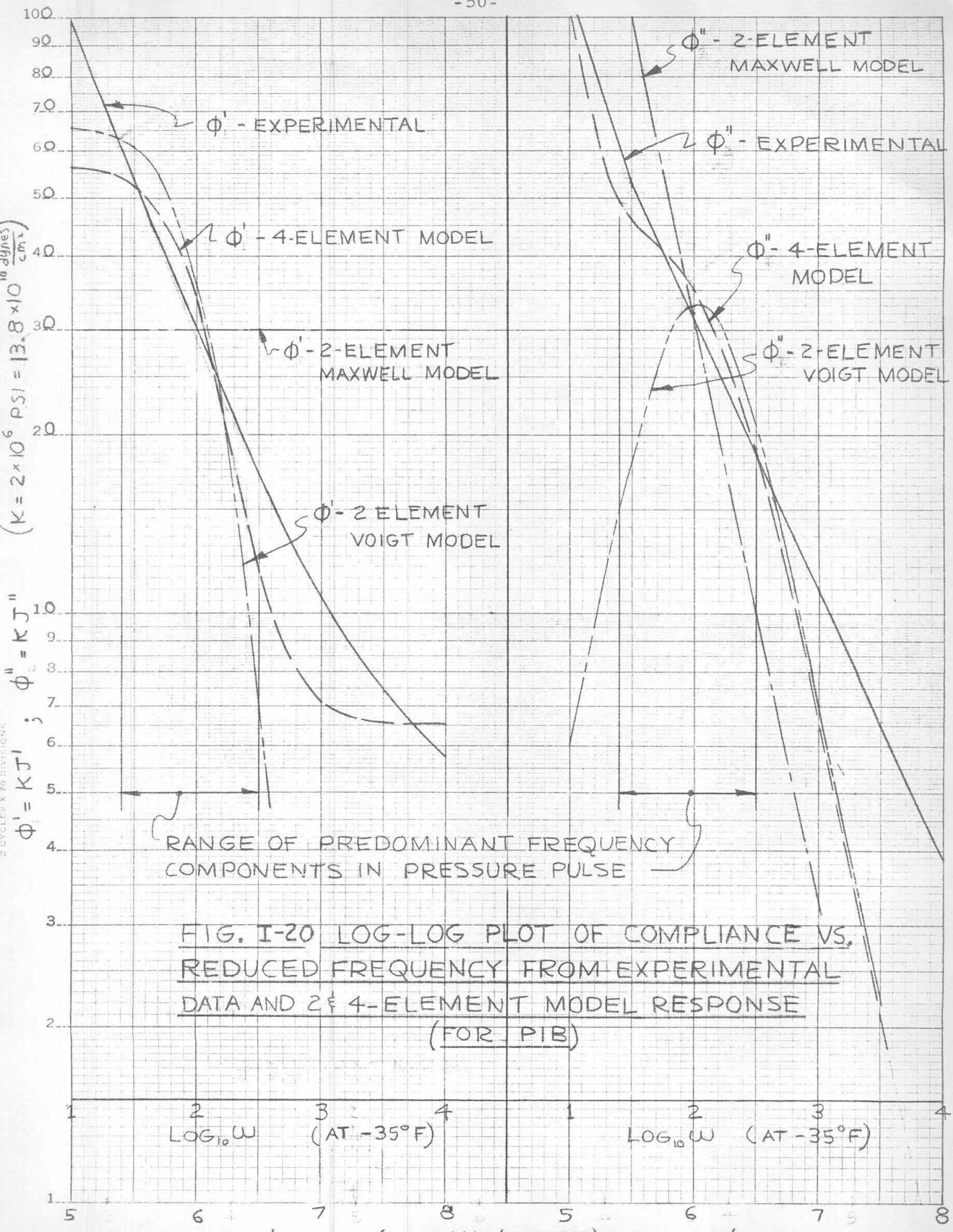

FIG. I-20 LOG-LOG PLOT OF COMPLIANCE VS. REDUCED FREQUENCY FROM EXPERIMENTAL DATA AND 2 & 4-ELEMENT MODEL RESPONSE (FOR PIB)

II. ELASTIC SOLUTIONS FOR CYLINDER

A. Pressure

6. Bond stresses for a bonded grain

In the fabrication of a large case-bonded solid propellant grain, it is often convenient to cast the grain in small sections, and to bond the sections sequentially in the chamber. Because of different elastic properties of bonding agent and propellant applied loading induces discontinuity stresses at the interface which may cause separation at or near the joint.

For the purpose of obtaining qualitative knowledge about the behavior of the system a model is studied: two semi-infinite sheets of thickness $2L$ (E_1, ν_1) are joined by a bonding material (E_2, ν_2) (cf. Fig. II-1); a pressure load is applied to the free surfaces.

Seidman[20] has attempted an approximate solution by way of the Ritz procedure, but obtained physically unreasonable results. The present paper obtains a solution by the method of restricted variation of the complementary energy.

a. Method of solution: If a product type approximation is chosen, the stresses

$$\sigma_x = f(x)\frac{d^2g(y)}{dy^2} + P_o$$

$$\sigma_y = \frac{d^2f(x)}{dx^2}\,g(y) \qquad (II-1)$$

$$\tau = -\frac{df(x)}{dx}\,\frac{dg(y)}{dy}$$

derived from the stress-function

$$\Phi = f(x)\,g(y) + \tfrac{1}{2}P_o y^2 \qquad (II-2)$$

in the conventional manner, are seen to satisfy equilibrium. The complementary energy may then be written in the form:

$$2E_2V^* = \int_{-\ell}^{\ell}\Big\{\int_{o}^{a}\left[(fg''+P_o)^2 + f''^2g^2 - 2\nu_2(fg''+P_o)f''g + 2(1+\nu_2)f'^2g'^2\right]dy$$

$$+ \frac{E_2}{E_1}\int_{a}^{\infty}\left[(fg''+P_o)^2 + f''^2g^2 - 2\nu_1(fg''+P_o)f''g + 2(1+\nu_1)f'^2g'^2\right]dy\Big\}dx \qquad (II-3)$$

---

*The primes denote differentiation with respect to the variable in question.

Performing the variation upon V* with respect to f(x) one obtains the differential equation

$$\frac{d^4 f}{dx^4} - 2A\frac{d^2 f}{dx^2} + Bf = -P_0 H \qquad (II-4)$$

where

$$A = \frac{\nu_2 \frac{E_1}{E_2}\int_0^a g g''dy + (1+\nu_2)\frac{E_1}{E_2}\int_0^a g'^2 dy + \nu_1 \int_a^\infty g g''dy + (1+\nu_1)\int_a^\infty g'^2 dy}{\frac{E_1}{E_2}\int_0^a g^2 dy + \int_a^\infty g^2 dy}$$

$$B = \frac{\frac{E_1}{E_2}\int_0^a g''^2 dy + \int_a^\infty g''^2 dy}{\frac{E_1}{E_2}\int_0^a g^2 dy + \int_a^\infty g^2 dy} \qquad (II-4a)$$

$$H = \frac{\frac{E_1}{E_2}\int_0^a g'' dy + \int_a^\infty g'' dy}{\frac{E_1}{E_2}\int_0^a g^2 dy + \int_a^\infty g^2 dy}$$

the solution of (4) is

$$f = C_1 \sinh\lambda_1 x + C_2 \cosh\lambda_1 x + C_3 \sinh\lambda_2 x + C_4 \cosh\lambda_2 x - \frac{1}{B}P_0 H \qquad (II-5)$$

with λ_1, λ_2 solutions of $\lambda^4 - 2A\lambda^2 + B = 0$.

b. Solution of the problem, g(y) assumed:

The function g(y) is to be chosen such that

i) g is an even function of y

ii) σ_y and τ vanish far from the discontinuity

iii) τ has a maximum at y = a;

(although it is not necessarily true that the maximum shear stress occurs at y = a, this assumption is made on intuitive grounds)

Three functions, each satisfying these conditions are

$$g_I = (1+\eta)e^{-\eta} \qquad (\eta = |y/a|) \qquad (II-6)$$

$$g_{II} = e^{-\frac{1}{2}\eta^2} \qquad (II-7)$$

$$g_{III} = 2-\eta^2 \qquad -1 \le \eta \le 1 \qquad (II-8)$$

$$= \frac{1}{\eta^2} \qquad \eta \le |1|$$

By comparing the energies and $\nabla^4\phi$(*) computed from these assumed functions, an estimate of the quality of the solutions may be found.

c. Numerical results:

Numerical calculations have been carried out for

$$\nu_1 = 0.5 \;, \quad \nu_2 = 0.3 \;, \quad E_1/E_2 = 0.1 \qquad \ell/a = 500$$

If one applies the boundary conditions

$$\sigma_x = P_0 \qquad \text{at } x = \pm \ell$$

$$\tau = 0 \qquad \text{at } x = \pm \ell$$

one arrives at the solution

$$f = \frac{P_0 H}{B}\left\{ \frac{\cosh\lambda_2 \frac{x}{\ell} - \frac{\lambda_2}{\lambda_1}\frac{\sinh\lambda_2}{\sinh\lambda_1}\cosh\lambda_1\frac{x}{\ell}}{\cosh\lambda_2 - \frac{\lambda_2}{\lambda_1}\frac{\sinh\lambda_2}{\sinh\lambda_1}\cosh\lambda_1} - 1 \right\} \qquad (\text{II}-9)$$

with the following values for H/b, λ_1, λ_2, and energies E**

Solution	I	II	III
λ_1	516.4	271.8	1352
λ_2	175.9	981.2	311.4
H/b	5.977	2.235	1.688
E	2.589	1.000	1.931

Hence, solution II is the most favorable one, solution I being the worst.

It is interesting to consider satisfaction of compatibility of displacements; as shown in Fig. II-4, solution I is better than solution II, and considerably better than solution III in this respect. Remembering, however, that the method does not attempt to satisfy compatibility but a minimum energy principle based on the stresses, this compatibility comparison does not invalidate the statement that solution II is the best of the three for estimating stresses.

The stresses along the interface (y = a, where separation may occur) are shown in Fig. II-3 for the three cases. Because of a scaling

---

* As $\nabla^4\phi = 0$ assures satisfaction of the compatibility condition, a comparison of $\nabla^4\phi$ will render a measure of how well compatibility is satisfied.

** As the sheet is infinite only the energy due to the presence of the bonding agent is considered. The energies are normalized with respect to that of the second solution.

problem, σ_x is not shown for case III: For $y = a(1-e)$, $(e \ll 1)$ σ_x rises from P_o at $x = L$ to $4.38\ P_o$ for $x \leq 0.97L$; for $y = a(1+e)$ σ_x drops from P_o at $x = L$ to $-9.12P_o$ for $x \leq 0.97L$.

d. Conclusion:

In conclusion, may it be repeated that the purpose of this paper is primarily to obtain qualitative knowledge about the stresses near the bond. Nevertheless it is felt that the result gives an idea of the magnitude of the strength required of the binder-propellant combination to prevent separation under a particular normal pressure.

As seen in Fig. II-3, the stress responsible for pull-away of propellant from binder, σ_y, is approximately equal to $2P_o$: therefore, if σ_y becomes greater than the tensile strength σ_u of the propellant or the bond strength, separation will occur, and hence an upper bound may be placed on the exerted pressure such that $P_o < \frac{1}{2}\sigma_u$.

Although it is in principle easy to determine mathematically the variations of the pressure bound with varying material constants, it appears algebraically simpler to recalculate the desired value for any particular case as outlined above.

NOTATION

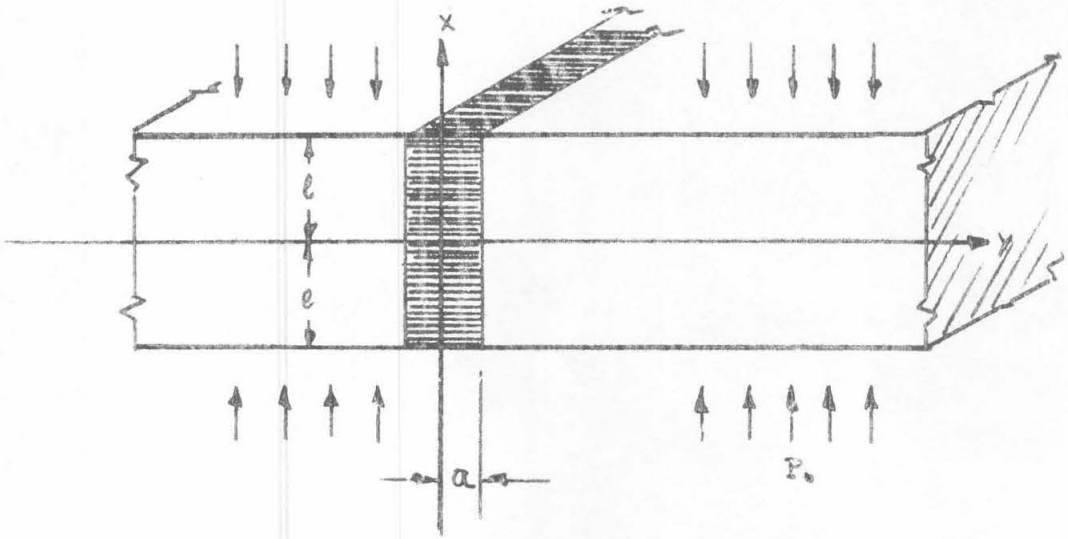

FIGURE II-1

$\eta = y/a$

P = SURFACE PRESSURE

REGION 1, E_1, ν_1 $\quad y > |a|$

REGION 2, E_2, ν_2 $\quad y < |a|$

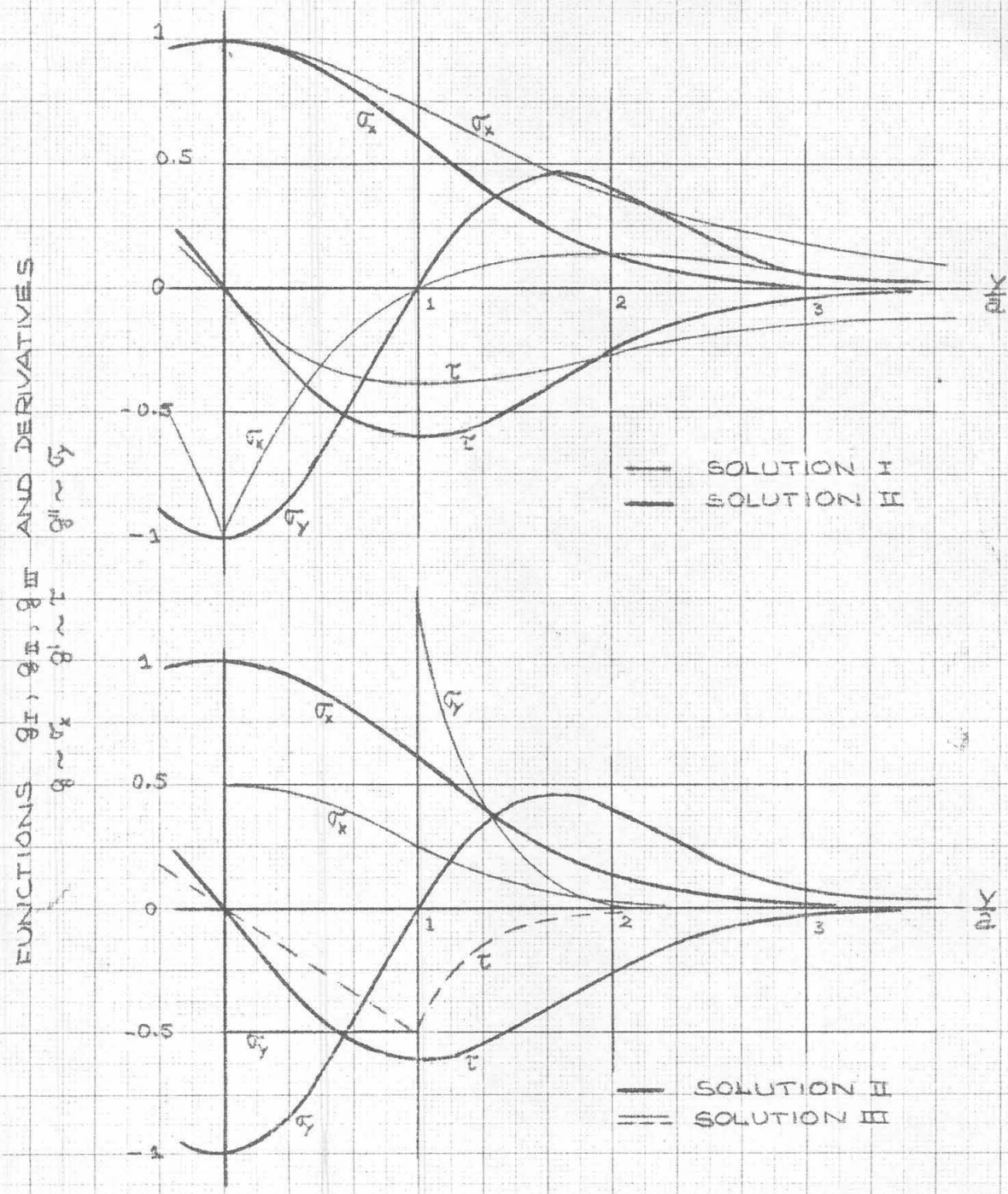

FIGURE II- 8

COMPARISON OF FUNCTIONS $g(y/2)$
(SYMBOLS INDICATE PROPORTIONALITY)

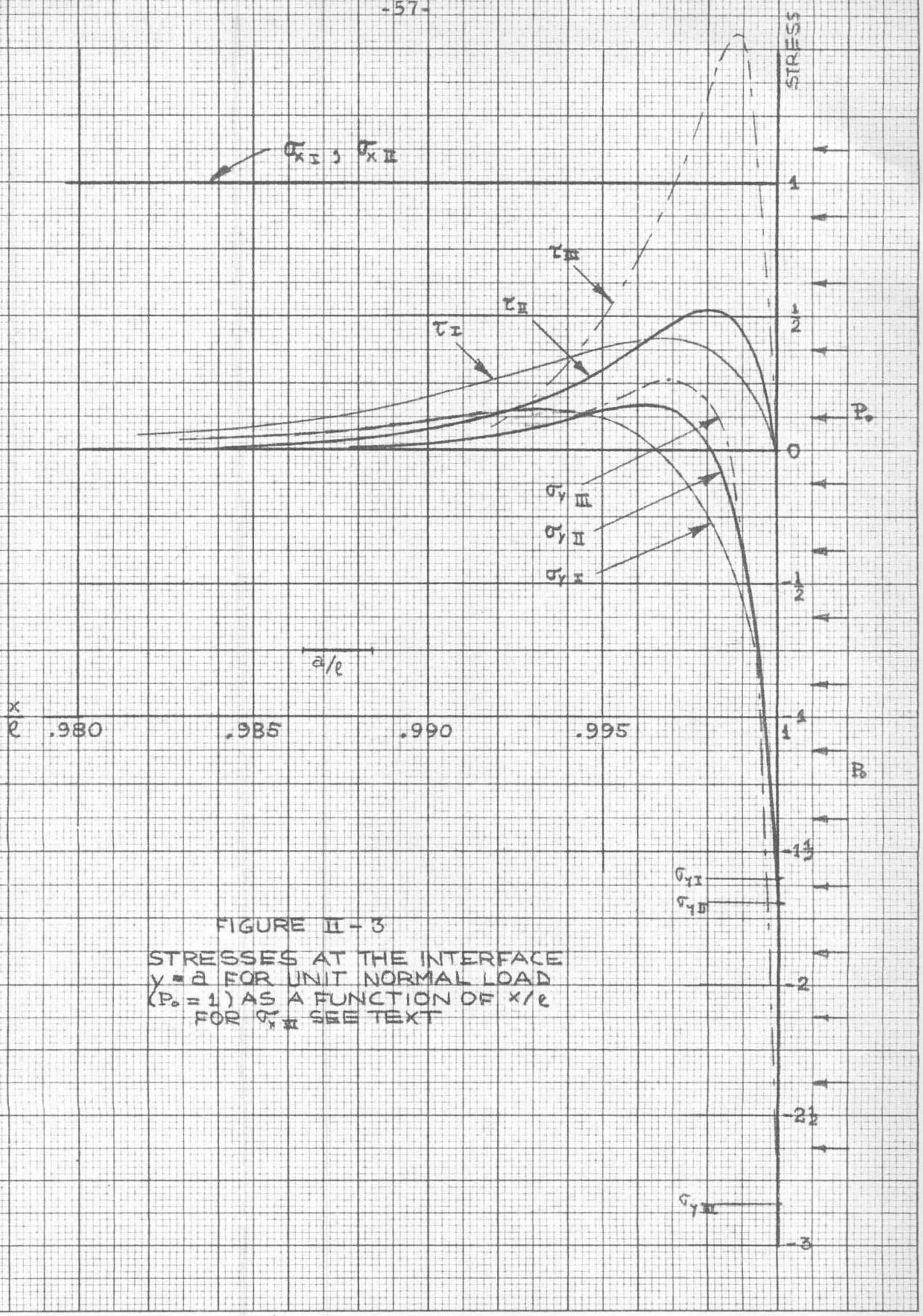

FIGURE II-3

STRESSES AT THE INTERFACE y = a FOR UNIT NORMAL LOAD ($P_o = 1$) AS A FUNCTION OF x/ℓ FOR $\sigma_{y\,III}$ SEE TEXT

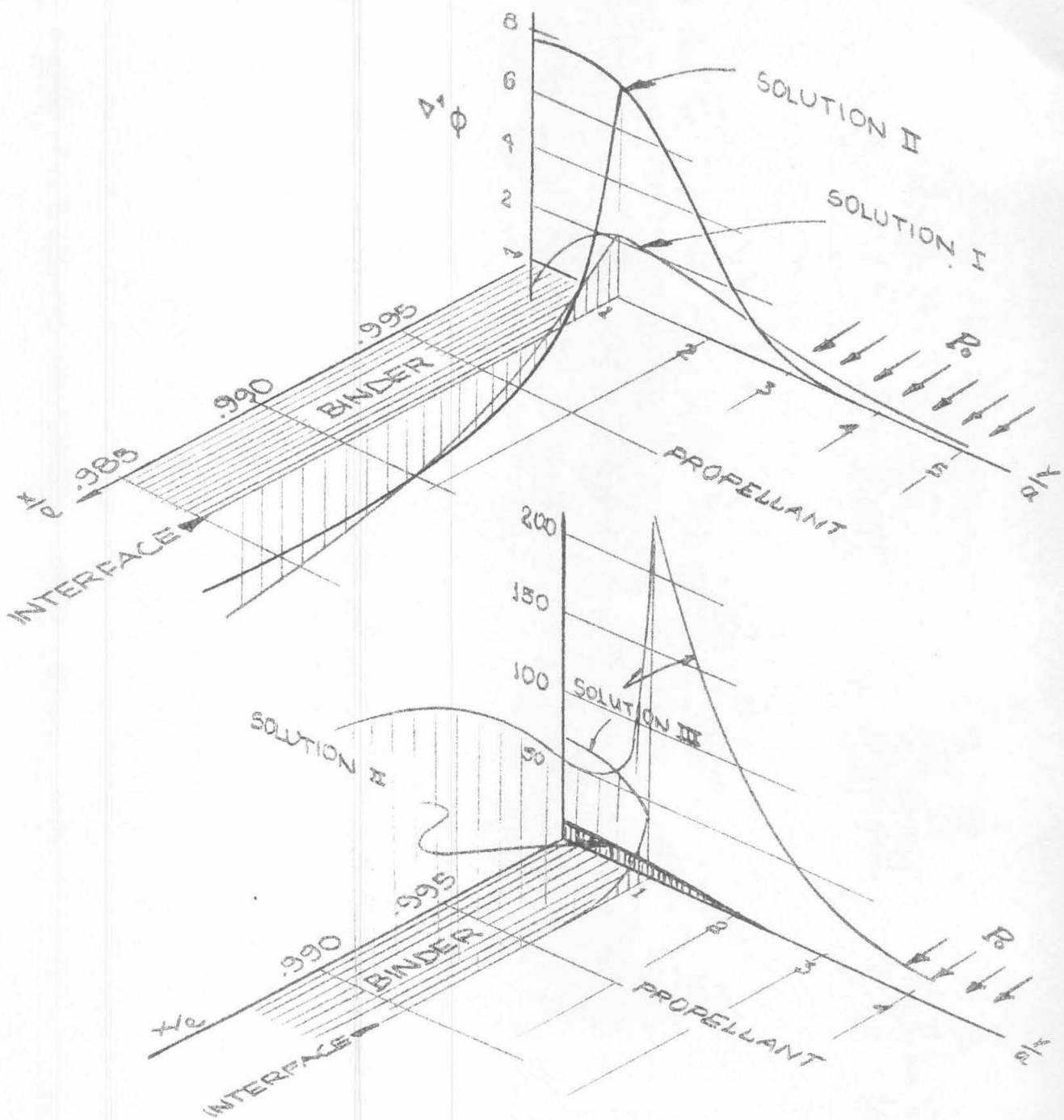

FIGURE II-4

$\Delta^4\phi$ AT $x = \ell$ & $y = a$

IV. ENGINEERING ANALYSIS

A. Viscoelastic pressure stresses for a cylinder at ignition.

Elastic solutions for pressurized cylinders have been given previously[10, 11] and subsequently extended to include the concentration effect present in star grains. In particular, the elastic solution for the star-point strain in a long case-bonded grain is given by equation (II-11b) in Progress Report No. 4 as

$$\epsilon_\theta^{SP} = \frac{1-\nu^2}{E}\left[-\left(\frac{1-2\nu}{1-\nu}\right) + K_L \frac{2\lambda^2}{\lambda^2-1}\left(1-\frac{P'}{P_i}\right)\right]P_i \qquad \text{(IV-1)}$$

where

$$\lambda = \frac{b}{a}$$

and all other symbols are defined in the above mentioned report. The pressure ratio $\frac{P'}{P_i}$ is given in Progress Report No. 1, page p-14:

$$\frac{P'}{P_i} = \frac{2(1-\nu^2)}{[1+\nu][1+(1-2\nu)\lambda^2] + (\lambda^2-1)(1-\nu_c^2)\frac{bE}{hE_c}} \qquad \text{(IV-2)}$$

Since the viscoelastic properties were given in the previous section I in terms of shear compliance ($J = \frac{1}{G}$) and bulk modulus (K), equations (IV-1) and (IV-2) will be rewritten in terms of these properties by using the relations given on page 7 of the first report.:

$$E = \frac{9KG}{3K+G} = \frac{9K}{3KJ+1} \qquad \text{(IV-3a)}$$

$$\nu = \frac{3K-2G}{2(3K+G)} = \frac{3KJ-2}{2(3KJ+1)} \qquad \text{(IV-3b)}$$

Substituting (IV-3) into (IV-2) and (IV-1), we obtain

$$\epsilon_\theta^{SP} = 1.5\frac{P_i}{K}\frac{\Phi}{(3\Phi+1)}\left\{-1 + 2K_i\lambda^2(1-\nu_c^2)C\,H(\Phi)\right\} \qquad \text{(IV-4)}$$

where we have defined $\Phi = KJ$, $C = \frac{bK}{hE_c}$,

$$H(\Phi) = \frac{\Phi^2\left[1+\frac{1}{2(1-\nu_c^2)C}\right] + \frac{5}{3}\Phi\left[1+\frac{2}{(1-\nu_c^2)5C}\right] + \frac{4}{9}}{\Phi^2 + 2\Phi\left[1+\frac{1+3\lambda^2}{6(\lambda^2-1)(1-\nu_c^2)C}\right](\lambda^2-1)(1-\nu_c^2)C + \frac{2}{3}(\lambda^2-1)(1-\nu_c^2)C} \qquad \text{(IV-5)}$$

Typical values for the various parameters are:

$$K = 2\times10^6 \text{ PSI}, \quad E_c = 30\times10^6 \text{ PSI}, \quad \nu_c = 0.3$$

$$\frac{b}{h} = 200, \quad \lambda = 2$$

from which C = 13.3.

It is observed that the terms containing (C) in the square brackets in $H(\phi)$ are quite small compared to unity if the above numbers are used. In fact, if they are neglected, $H(\phi)$ reduces to

$$H(\phi) = \frac{\phi + \frac{4}{3}}{\phi + 2(\lambda^2-1)(1-\nu_c^2)C} = \frac{\phi + 1.33}{\phi + 72.80} \qquad \text{(IV-6)}$$

If 4/3 is neglected compared to ϕ, the incompressible limit case results after elimination of K from (IV-4). However further analysis will show that for short times, when ϕ is small, the 4/3 term should be retained. If all terms are retained in (IV-5) we find

$$H(\phi) = 1.04\,\frac{(\phi+1.33)(\phi+0.320)}{(\phi+76.82)(\phi+0.316)} \doteq 1.04\,\frac{\phi+1.33}{\phi+76.82} \qquad \text{(IV-7)}$$

so that both the numerator and denominator again become first order in ϕ. This has particular significance in reducing the complexity of the viscoelastic problem in which ϕ is a differential operator. Using the approximate expression for $H(\phi)$ from (IV-7), the star-point strain is

$$\epsilon_\theta^{SP} = 0.75\,\frac{\phi}{(3\phi+1)}\left\{-1 + 101\,K_i\left[\frac{\phi+1.33}{\phi+76.82}\right]\right\} P_i \times 10^{-6} \qquad \text{(IV-8)}$$

Since ϕ is proportional to the grain's compliance, its limiting values are given by the material's long time (or zero frequency) value and the short time (or infinite frequency) value. From the PIB data in Fig. I-17 of Material Behavior section, the largest possible value for ϕ is

$$\phi(\omega=0) = KJ(\omega=0) = 1.38\times10^4 \qquad \left(K = 13.8\times10^{10}\,\frac{\text{dynes}}{\text{cm}^2}\right)$$

and the smallest (IV-9)

$$\phi(\omega=\infty) = KJ(\omega=\infty) = 4.36$$

Because the minimum value of ϕ is 4.36, the term (-1) will be neglected in (IV-8), and also we will let

$$\frac{\Phi}{3\Phi+1} \doteq \frac{1}{3}$$

With these reasonable approximations, the strain is

$$\epsilon_\theta^{SP} \doteq 25 K_i \left[\frac{\Phi + 1.33}{\Phi + 76.82}\right] P_i \times 10^{-6} \qquad \text{(IV-10)}$$

Without carrying out a viscoelastic analysis the minimum and maximum values of ϵ_θ^{SP} can be found for a pressure step P_i applied at t = o and held constant indefinitely. The initial strain is given by substituting ϕ = 4.36 into(IV-10),

$$\epsilon_\theta^{SP}(t=0) \doteq 1.75 K_i P_i \times 10^{-6}$$

and the long time strain is given by using $\Phi = 1.38 \times 10^4$ in (IV-10)

$$\epsilon_\theta^{SP}(t=\infty) \doteq 25 K_i P_i \times 10^{-6}$$

It is important to recognize that these limiting values of strain do not, in general, provide sufficient information to predict whether or not the grain will fail upon ignition; the failure criterion will depend upon the entire strain history and hence the way in which ϵ_θ^{SP} varies with time.

To illustrate the various procedures, examples will be presented showing the determination of time dependent responses for ramp type pressure inputs typical of an ignition loading for a propellant grain. First, discrete-element models will be employed, followed by an exact solution in order to examine the accuracy of the models and to investigate the practicability of bypassing models entirely by using the Fourier inversion integral technique.

3. Ramp pressure rise, bulk elasticity, discrete-element model.

The strain will be found first for a unit pressure step and then this solution will be used to find the response for the ramp type pulse discussed previously. With viscoelasticity, we look upon ϕ (IV-10) as being a differential operator consisting of time derivatives $P \equiv \frac{d}{dt}$. For convenience we write (IV-10) as

$$\epsilon_o^{sp} = 25\, K_i \times 10^{-6}\, \xi(t) \qquad \text{(IV-11)}$$

and define $\xi(t)$ as the normalized strain due to a unit pressure step $S_i(t)$ applied at t = o:

$$\xi(t) = \frac{\phi(p) + 1.33}{\phi(p) + 76.82} S_i(t) \qquad \text{(IV-12)}$$

$\xi(t)$ will be found first using a four-element model. Recall that

$$\phi(p) = K\, J(p)$$

and that J(p) is given by the operational compliance k(p) in Fig. I-12a

$$\phi(p) = K\left[J_g + \frac{1}{\eta p} + \frac{J_1}{\tau_1 p + 1} \right]$$

Using the same definitions given in the section I-B

$$\beta_g = K J_g \quad , \quad \beta_1 = K J_1 \quad , \quad \beta_2 = \frac{K \tau_1}{\eta}$$

we have

$$\phi(p) = \beta_g + \frac{\beta_1}{\tau_1 p + 1} + \frac{\beta_2}{\tau_1 p} \qquad \text{(IV-13)}$$

Substitution of (IV-13) in (IV-12) yields

$$\xi(t) = \frac{(\beta_g + 1.33)p^2 + \left(\beta_1 + \beta_2 + \beta_g + 1.33\right)\frac{p}{\tau_1} + \frac{\beta_2}{\tau_1^2}}{(\beta_g + 76.82)p^2 + \left(\beta_1 + \beta_2 + \beta_g + 76.82\right)\frac{p}{\tau_1} + \frac{\beta_2}{\tau_1^2}} S_i(t) \qquad \text{(IV-14)}$$

Substituting the model parameters

$$\beta_1 = 50 \qquad \beta_2 = 9.5 \qquad \beta_g = 6.5 \qquad \tau_1 = .925 \times 10^{-2} \text{ Sec}$$

into (IV-14) and then factoring the denominator, $\xi(t)$ becomes

$$\xi(t) = 0.094 \frac{P^2 + 9.3 \times 10^2 P + 1.42 \times 10^4}{(P+7.5)(P+177.5)} S_i(t) \qquad \text{(IV-15)}$$

The unit pressure step is defined as:

$$S_i(t) = 0 \qquad t < 0$$
$$S_i(t) = 1 \qquad t > 0 \qquad \text{(IV-16)}$$

and the grain is assumed to be unstrained initially:

$$\xi(t) = 0 \qquad t < 0 \qquad \text{(IV-17)}$$

The differential equation (IV-15) can be integrated directly by partial fractions or else by Laplace transform in which p is the transform variable,

$$\overline{S_i}(P) = \frac{1}{P}$$

the transformed pressure, and

$$\bar{\xi} = 0.094 \frac{P^2 + 9.3 \times 10^2 P + 1.42 \times 10^4}{(P+7.5)(P+177.5)} \frac{1}{P} \qquad \text{(IV-18)}$$

the transformed strain. The time dependent normalized strain is found as

$$\xi(t) = 1 - 0.54 e^{-7.5t} - 0.37 e^{-177.5t} \qquad \text{(IV-19)}$$

which is plotted in Fig. IV-1 for three different time scales. The behavior of ξ for short times, $0 < t < 0.01$, is governed by the second exponential in (IV-19); while the relatively long time behavior, $t > 0.03$, is determined by the first exponential. It is interesting to see that the time interval in which both exponentials act is in the time scale of the pressure pulse.

The time dependence resulting when the two-element models are used is found in a similar fashion. From Fig.I-10 , the operational shear compliance for the Voigt model is

$$\Phi(P) = \frac{K J_v}{\tau_v P + 1} = \frac{\beta_v}{\tau_v P + 1} \qquad \text{(IV-20)}$$

and for the Maxwell model is

$$\Phi(P) = K \left[J_m + \frac{J_m}{\tau_m P} \right] = \beta_m + \frac{1}{\beta P} \qquad \text{(IV-21)}$$

Substituting (IV-20) and (IV-21) into the normalized strain $\xi(t)$, equation (IV-12), we find for the Voigt model

$$\xi(t) = 0.017 \left[\frac{P + \dfrac{\beta_v + 1.33}{1.33\,\tau_v}}{P + \dfrac{\beta_v + 76.82}{76.82\,\tau_v}} \right] S_c(t) \qquad \text{(IV-22)}$$

and for the Maxwell model

$$\xi(t) = \left[\frac{\beta_m + 1.33}{\beta_m + 76.82} \right] \left[\frac{P + \dfrac{1}{\beta(\beta_m + 1.33)}}{P + \dfrac{1}{\beta(\beta_m + 76.82)}} \right] S_c(t) \qquad \text{(IV-23)}$$

Integration of (IV-22) using the unit pressure step (IV-16) yields for the Voigt model:

$$\xi(t) = 0.47 - 0.45\, e^{-201\,t} \qquad \text{(IV-24)}$$

in which we have used the previously determined parameter values of $\beta_v = 66$, and $\tau_v = 0.925 \times 10^{-2}$ seconds.
Similarly, from (IV-23) we find the response for the Maxwell model:

$$\xi(t) = 1 - 0.71 e^{-30t} \tag{IV-25}$$

in which we have set $\beta_m = 30$ and $\beta = 0.312 \times 10^{-3}$ seconds.

The response curves shown in Fig. IV-1 for both two-element models clearly indicate that a four-element model is needed to obtain sufficient accuracy for times of the order of the pressure rise time, 0.01 seconds.

Strain response to the unit pressure step can be used to calculate the response $\psi(t)$ to an arbitrary pressure loading $p_i(t)$ by using the Duhamel integral[19]:

$$\psi(t) = \int_0^t \xi(t-u) \frac{dp_i(u)}{du} du \tag{IV-26}$$

in which the pressure is assumed to vanish for $t < 0$. The star point strain follows from equation (IV-10):

$$\epsilon_\theta^{sp} = 25 K_i \times 10^{-6} \psi(t) \tag{IV-27}$$

We will now specialize (IV-26) to the ramp type pulse illustrated in Fig. IV-2 with a derivative defined mathematically as

$$\begin{aligned}
\frac{dp_i}{dt} &= 0 && t<0 \\
\frac{dp_i}{dt} &= \frac{p_0}{t_1} && 0<t<t_1 \\
\frac{dp_i}{dt} &= 0 && t_1<t<t_2 \\
\frac{dp_i}{dt} &= -\frac{p_0}{t_1} && t_2<t<t_1+t_2 \\
\frac{dp_i}{dt} &= 0 && t_1+t_2<t
\end{aligned} \tag{IV-28}$$

Using the pressure derivative given by (IV-28) $\psi(t)$ becomes

$$\psi(t) = \frac{P_0}{t_1}\int_0^t \xi(u)\,du \qquad 0 < t < t_1 \qquad \text{(IV-29a)}$$

$$\psi(t) = \frac{P_0}{t_1}\int_{t-t_1}^t \xi(u)\,du \qquad t_1 < t < t_2 \qquad \text{(IV-29b)}$$

$$\psi(t) = \frac{P_0}{t_1}\left\{\int_{t-t_1}^t \xi(u)\,du - \int_0^{t-t_2} \xi(u)\,du\right\} \qquad t_2 < t < t_1+t_2 \qquad \text{(IV-29c)}$$

$$\psi(t) = \frac{P_0}{t_1}\left\{\int_{t-t_1}^t \xi(u)\,du - \int_{t-(t_1+t_2)}^{t-t_2} \xi(u)\,du\right\} \qquad t_1+t_2 < t \qquad \text{(IV-29d)}$$

The response for the three different models, obtained by substituting (IV-19), (IV-24), and (IV-25) into equations (IV-29), is shown by Fig. IV-2.

It will be recalled that in the spectral analysis we assumed that most of the strain due to one entire pulse would relax out by the time $t = 12t_1 = 0.12$ seconds. It is seen from the four-element curve that this assumption is valid since only about $10^{\circ}/o$ of the maximum value remains at $t = 12t_1$.

It is important to recognize that the model parameters used in the foregoing analysis are functions of both temperature and time scale of the pressure pulse. More precisely, the parameters depend on where the frequency band of interest lies on the master curve of dynamic data. In order to make a complete design study for various temperatures and pressure rise times, it is necessary to first determine the model parameters as a function of position of this band. Then for each specified pressure rise time and temperature, the appropriate frequency band must be found. However, with each model the grain and case geometry can be varied independently of the model parameters. This assumes, of course, that the strain occuring with the various geometries relaxes out sufficiently rapid in order that the spectral analysis is valid.

4. Ramp pressure rise, bulk elasticity, direct incorporation of complex compliance test data.

As an alternative method of analysis, an exact solution to the viscoelastic problem can be obtained by using experimental values for dynamic data directly in the Fourier inversion integral. In view of the data existing only in graphical form, it is necessary to use numerical integration. It turns out that it is much easier to perform the numerical inversion if the pressure is a step function rather than a pulse associated with a particular time scale. Thus, we will first determine the strain for a pressure step applied at t = o, and then extend the results to the ramp pressure by using equations (IV-29).

The expression for strain (IV-12), is actually a differential equation in which the exact form of the operator $\phi(p)$ is unknown. By using finite-element models, as in the previous section, this operator is approximated by a low order polynomial in p. The precise form of $\phi(p)$ can usually be found by utilizing an infinite-element model which is discussed under Model Theory in this report. However, application of the Fourier transform and inversion integral enables the strain to be found without using model theory wherein only the assumption of linear viscoelastic response is required. The Fourier transform of a function f(t) is defined as

$$\bar{f}(\omega) = \int_{-\infty}^{\infty} f(t)\, e^{-i\omega t}\, dt \qquad \text{(IV-30)}$$

with the inversion integral

$$f(t) = \frac{1}{2\pi} \int_{-\infty}^{\infty} \bar{f}(\omega)\, e^{i\omega t}\, d\omega \qquad \text{(IV-31)}$$

Formally operating on the differential equation (IV-12) with the transform is equivalent, with zero initial conditions, to replacing the time derivative p by iw and the pressure $S_i(t)$ by $\overline{S_i}(w)$; therefore

$$\overline{\xi}(\omega) = A(\omega)\, \overline{S_i}(\omega) \qquad \text{(IV-32)}$$

where the complex admittance A(w) is defined as

$$A(\omega) = \frac{\Phi(i\omega) + 1.33}{\Phi(i\omega) + 76.82} \tag{IV-33}$$

However, $\phi(iw)$ is actually the nondimensional complex compliance, $\phi^*(w)$, defined previously as

$$\Phi(i\omega) = \Phi^*(\omega) = K J^*(\omega) = \Phi'(\omega) - i\,\Phi''(\omega)$$

$$\Phi'(\omega) = K J'(\omega) \quad ; \quad \Phi''(\omega) = K J''(\omega)$$

Substituting $\phi(iw) = \phi'(w) - i\phi''(w)$ into A(w) and rearranging to form the real and imaginary components we find

$$A(\omega) = A_1(\omega) - i\,A_2(\omega) \tag{IV-34}$$

where

$$A_1(\omega) = \frac{(\Phi')^2 + (\Phi'')^2 + 78.15\,\Phi' + 102.5}{(\Phi')^2 + (\Phi'')^2 + 153.6\,\Phi' + 5900} \tag{IV-35}$$

$$A_2(\omega) = \frac{75.5\,\Phi''}{(\Phi')^2 + (\Phi'')^2 + 153.6\,\Phi' + 5900} \tag{IV-36}$$

It will be convenient to write A(w) in an alternative form

$$A(\omega) = |A(\omega)|\, e^{-i\epsilon(\omega)} \tag{IV-37}$$

where

$$|A(\omega)| = \sqrt{A_1^2(\omega) + A_2^2(\omega)}$$

$$\epsilon(\omega) = \tan^{-1} \frac{A_2(\omega)}{A_1(\omega)}$$

Both (IV-34) and (IV-37) are plotted in Fig. IV-3 by using values for ϕ' and ϕ'' taken directly from the master curves of the real and imaginary components of complex compliance.

We have defined $\overline{S_i}(w)$ as the transform of a unit step function which vanishes for $t < o$ and equals unity for $t > o$. However the transform cannot be found directly since the transform of the step from (IV-30) is

$$\int_o^\infty e^{-iwt}\,dt$$

which does not converge to a definite limit. Consequently we must consider a modified step function

$$\begin{aligned} S_\gamma(t) &= 0 \qquad && t<0 \\ S_\gamma(t) &= e^{-\gamma t} \qquad && t>0 \end{aligned} \tag{IV-38}$$

and let $\gamma \to o$ after the final form of the inversion integral is determined. It is shown in the following that γ can be taken identically as zero in the portion of the inversion integral requiring numeral integration, while the portion in which we cannot initially take it as zero can be evaluated analytically. The transform of (IV-38) is given by (IV-30) as

$$\overline{S_\gamma}(\omega) = \int_o^\infty e^{-t(\gamma+i\omega)}\,dt = \frac{1}{\gamma+i\omega} \tag{IV-39}$$

From (IV-31) and (IV-39) the normalized strain due to a unit pressure step is written formally as

$$\xi(t) = \frac{1}{2\pi} \lim_{\gamma\to o} \int_{-\infty}^{\infty} A(\omega)\,\overline{S_\gamma}(\omega)\,e^{i\omega t}\,d\omega \tag{IV-40}$$

$$= \frac{1}{2\pi} \lim_{\gamma\to o} \int_{-\infty}^{\infty} \frac{A(\omega)}{\gamma+i\omega}\,e^{i\omega t}\,d\omega$$

In order to numerically integrate (IV-40), it must first be written as a real integral. It is convenient to use form (IV-37) for $A(\omega)$ so that

$$A(\omega)\, e^{i\omega t} = |A|\, e^{i(\omega t - \epsilon)} = |A|\left[\cos(\omega t - \epsilon) + i \sin(\omega t - \epsilon)\right] \tag{IV-41}$$

Substituting (IV-41) into (IV-40) and writing

$$\frac{1}{\gamma + i\omega} = \frac{\gamma - i\omega}{\gamma^2 + \omega^2}$$

we find

$$\varphi(t) = \frac{1}{2\pi} \lim_{\gamma \to 0} \int_{-\infty}^{\infty} \frac{|A|}{\gamma^2 + \omega^2} [\gamma - i\omega][\cos(\omega t - \epsilon) + i \sin(\omega t - \epsilon)]\, d\omega \tag{IV-42}$$

ϵ has been defined as

$$\epsilon = \tan^{-1} \frac{A_2(\omega)}{A_1(\omega)}$$

in which A_2 and A_1 are known only for $\omega > 0$. However, behavior of ϵ for negative ω can be determined from model theory. Reference to the most general model given in Figs. (I-14) or (I-15) shows that the real component of complex compliance is even in ω, and the imaginary component is odd in ω. Thus, from (IV-35) and (IV-36) it is clear that $|A|$ is an even function while ϵ is odd. Using this fact we can write (A-42) as two real integrals with limits from 0 to ∞:

$$\varphi(t) = \frac{1}{\pi} \lim_{\gamma \to 0} \int_{0}^{\infty} \frac{|A|\, \omega \sin(\omega t - \epsilon)}{\gamma^2 + \omega^2}\, d\omega$$

$$+ \frac{1}{\pi} \lim_{\gamma \to 0} \gamma \int_{0}^{\infty} \frac{|A| \cos(\omega t - \epsilon)}{\gamma^2 + \omega^2}\, d\omega = I_1 + I_2 \tag{IV-43}$$

The first integral, defined as I_1, converges uniformly for all γ and hence we can set $\gamma = 0$ under the integral sign. It is seen that if we set $\gamma = 0$ in the second integral I_2 it diverges due to the $\frac{1}{\omega^2}$ term in the integrand and the lower limit being zero. However, a change of variable will allow the limit to be taken. Letting $\omega \to \gamma\Omega$ in I_2, we obtain

$$I_2 = \frac{1}{\pi} \lim_{\gamma \to 0} \int_{0}^{\infty} \frac{|A(\gamma\Omega)|}{1 + \Omega^2} \cos\left(\gamma\Omega t - \epsilon(\gamma\Omega)\right) d\Omega \tag{IV-44}$$

Since I_2 is uniformly convergent in γ, we may set $\gamma = 0$ under the integral sign, thus:

$$I_2 = \frac{1}{\pi} |A(0)| \int_0^\infty \frac{d\Omega}{1+\Omega^2} = \frac{1}{2} \qquad \text{(IV-45)}$$

in which we have used the fact that

$$|A(0)| = 1 \quad , \quad \epsilon(0) = 0$$

Therefore $\xi(t)$ in (IV-43) is given by

$$\xi(t) = \frac{1}{\pi} \int_0^\infty \frac{|A|}{\omega} \sin(\omega t - \epsilon) d\omega + \frac{1}{2} \qquad \text{(IV-46)}$$

If the transform of the pressure had initially been taken as $\frac{1}{i\omega}$, rather than $\frac{1}{\gamma + i\omega}$, only the integral in (IV-46) would have been obtained.

$\xi(t)$ can now be found by numerical integration of (IV-46). The method employed for the problem in this report was to use Simpson's rule for approximately the first two cycles of sin (wt- ϵ), and then construct analytical approximations for the remaining range of integration in which the contribution to $\xi(t)$ was relatively small.

The result is plotted on log-log paper in Fig. IV-4, and for three different times scales in Fig. IV-1 indicated as the "exact" response. The strain can be approximated by a few straight lines on log-log paper so that it has a power law form as shown in Fig. IV-4.

A very useful approximate relation exists between the real part of the admittance A_1 and the strain $\xi(t)$. Examination shows that

$$\xi\left(\frac{0.5}{\omega}\right) \doteq A_1(\omega) \tag{IV-47}$$

Thus, by taking values of $A_1(w)$ from Fig. IV-3 and plotting these values against $t = \frac{0.5}{w}$, a good approximation to the exact normalized strain is obtained as shown in Fig. IV-4. It is expected that this "rule" will hold as long as the complex admittance has the form shown in Fig. IV-3; however, other examples should be examined in order to determine the generality of the rule.

The solution $\xi(t)$ was obtained for a particular geometry in which certain dimensions were assumed. If it is desired to study the response as a function of dimensional changes, in principle, the complete Fourier inversion must be carried out with each set of dimensions. However, if the rule

$$\xi\left(\frac{\alpha}{\omega}\right) \doteq A_1(\omega) \tag{IV-48}$$

is found to hold for one set of dimensions, the strain can be computed directly from (IV-48) when other sets are used. In the problem just solved $\alpha = 0.5$; however, it may be somewhat different for various materials and may change significantly if radical changes in dimensions are made. In a design study involving dimensional changes, limiting values should be used to check the value for α.

The analytical approximations to $\xi(t)$, given in Fig. IV-4, were substituted directly into equations (IV-29) in order to calculate the normalized strain response for the pressure pulse shown in Fig. IV-2. The elastic limit cases for the strain are shown as well as the actual viscoelastic response. The limit cases correspond to the hypothetical

situations in which the grain responds with glassy compliance (the smallest possible compliance which is the limiting value at high frequency) and the rubbery or equilibrium compliance (the largest possible compliance which is the limiting value at low frequencies). It is clearly seen that the actual strain history is considerably different than an elastic limit analysis would indicate.

It is important to recognize that it was not necessary to specify any pressure time scale or temperature in obtaining the fundamental solution $\xi(t)$. This was necessary with the finite-element model analysis and consequently the solutions were valid only for a specified time scale and temperature. Since the solution just obtained is known for all time, (the very short time portion is not shown in Fig. IV-4, however it can be found from the inversion integral) it can be used to draw a master response curve which is valid as long as the material's temperature is constant in time. That is, the time-temperature superposition principle discussed in the Model Theory section can be applied by plotting ξ as a function of $(\frac{t}{a_T})$. It should be recalled that a small approximation is made in doing this since the linear dependence of compliance on temperature has been neglected. If this dependency is considered, then the admittance plotted against reduced frequency (wa_T) will change slightly with temperature. However, the present inaccuracy of propellant data does not warrant such a correction.

The master curve for $\xi\,(\frac{t}{a_T})$ can be used to make a parametric study of response as a function of temperature and pressure rise time for each set of dimensions assigned to the grain-case geometry. In view of the imperical relation found between the real part of the admittance A_1 and ξ, namely

$$\xi(t) \doteq \xi\left(\frac{\alpha}{\omega}\right) \doteq A_1(\omega) \qquad \text{(IV-48)}$$

or in terms of reduced variables

$$\xi\left(\frac{t}{a_T}\right) \doteq \xi\left(\frac{\alpha}{\omega a_T}\right) \doteq A_1(\omega a_T) \qquad \text{(IV-49)}$$

the response $\xi\left(\frac{t}{a_T}\right)$ can be found quite readily as a function dimensions if further examination verifies the relation for other examples. Such a set of master curves would allow a complete design study to be made. This conclusion may be contrasted with that made for the solution with finite-element models. Namely, it was pointed out that each solution could be used in a parameteric study in which dimensions changed, while a set of these were needed to study the effect of temperature and pressure pulse variations. The particular application should dictate which solution is most useful.

FIG. IV-1 TIME DEPENDENCE OF NORMALIZED STRAIN AT STAR POINT DUE TO UNIT PRESSURE STEP APPLIED AT t=0 (FOR PIB AT -35°F)

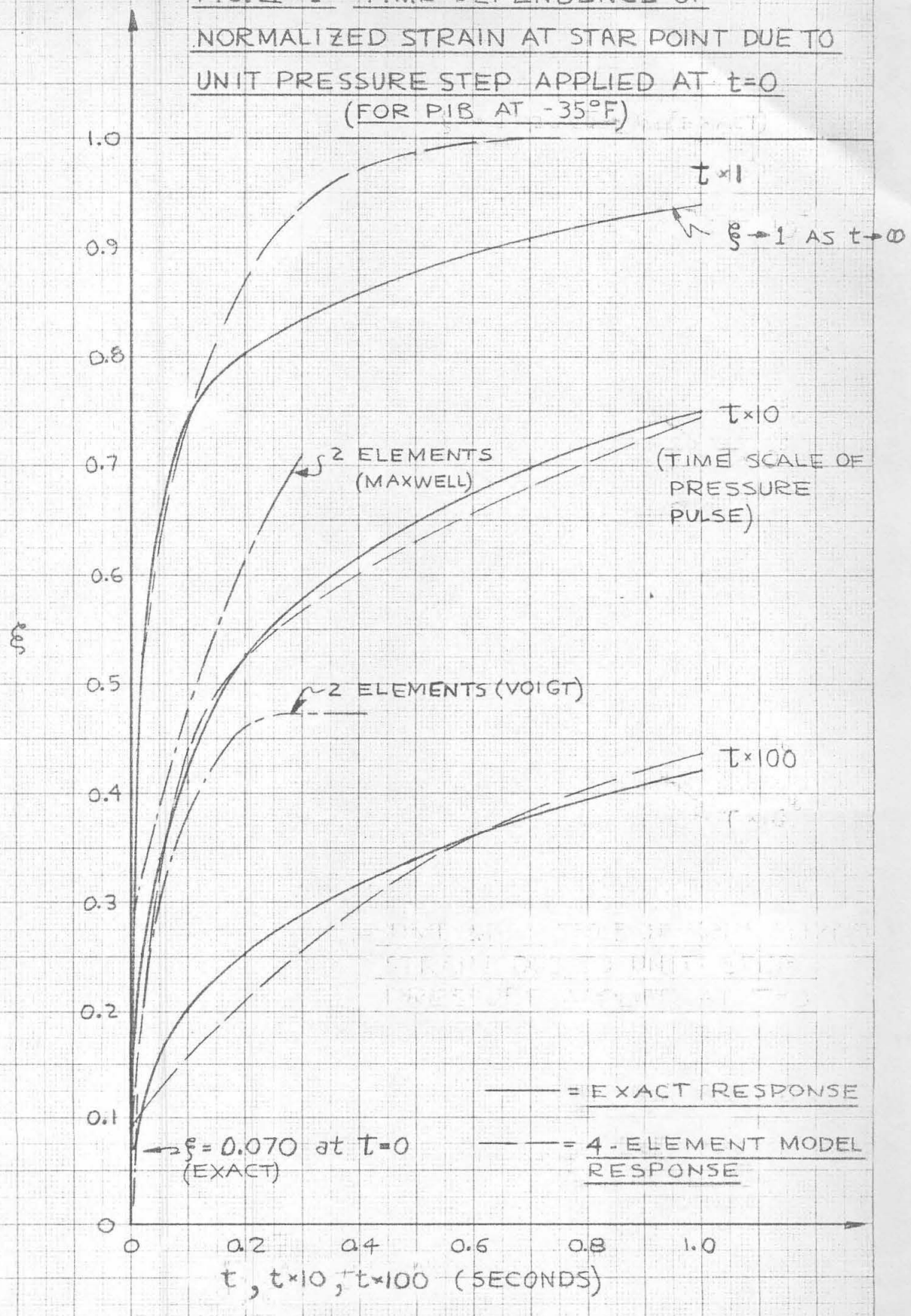

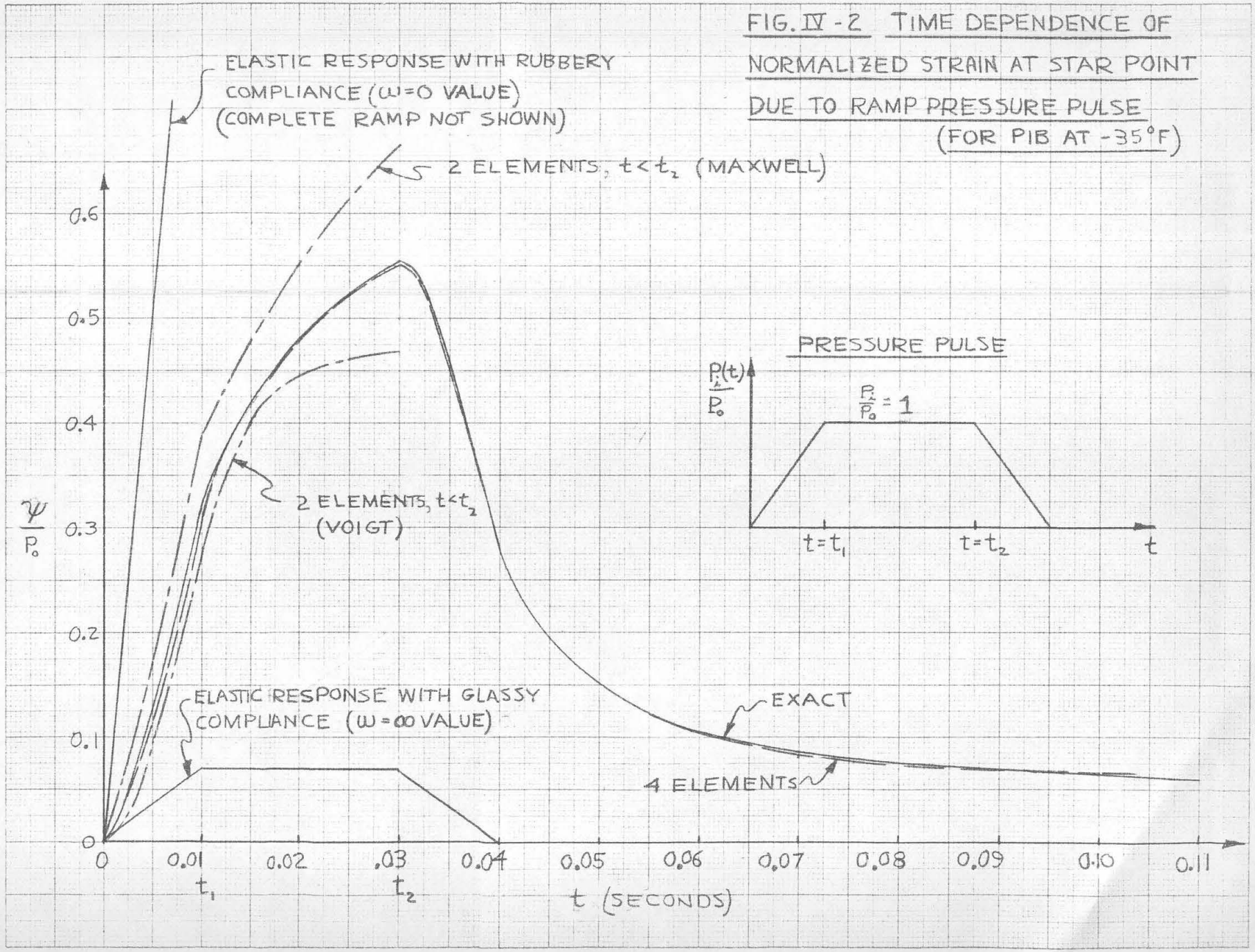
FIG. IV - 2 TIME DEPENDENCE OF NORMALIZED STRAIN AT STAR POINT DUE TO RAMP PRESSURE PULSE (FOR PIB AT -35°F)
ELASTIC RESPONSE WITH RUBBERY COMPLIANCE (ω=0 VALUE)
(COMPLETE RAMP NOT SHOWN)
2 ELEMENTS, t<t₂ (MAXWELL)
2 ELEMENTS, t<t₂ (VOIGT)
ELASTIC RESPONSE WITH GLASSY COMPLIANCE (ω=∞ VALUE)
EXACT
4 ELEMENTS
PRESSURE PULSE
P(t)/P₀
P/P₀ = 1
t=t₁
t=t₂
t
ψ/P₀
0.6
0.5
0.4
0.3
0.2
0.1
0
0.01
0.02
.03
0.04
0.05
0.06
0.07
0.08
0.09
0.10
0.11
t₁
t₂
t (SECONDS)

FIG. IV-3 COMPLEX ADMITTANCE FOR STRAIN AT STAR POINT IN CASE-BONDED GRAIN (FOR PIB)

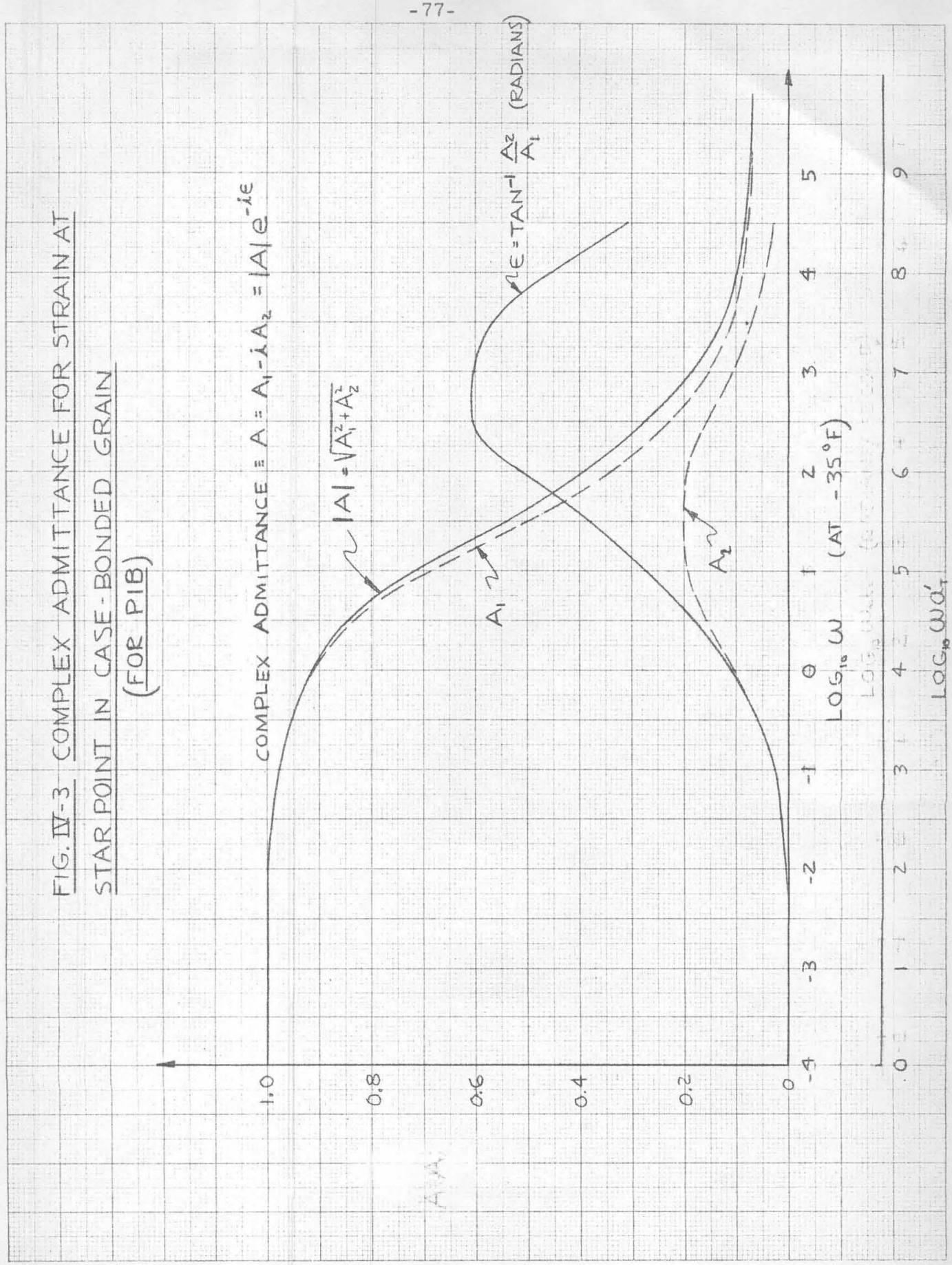

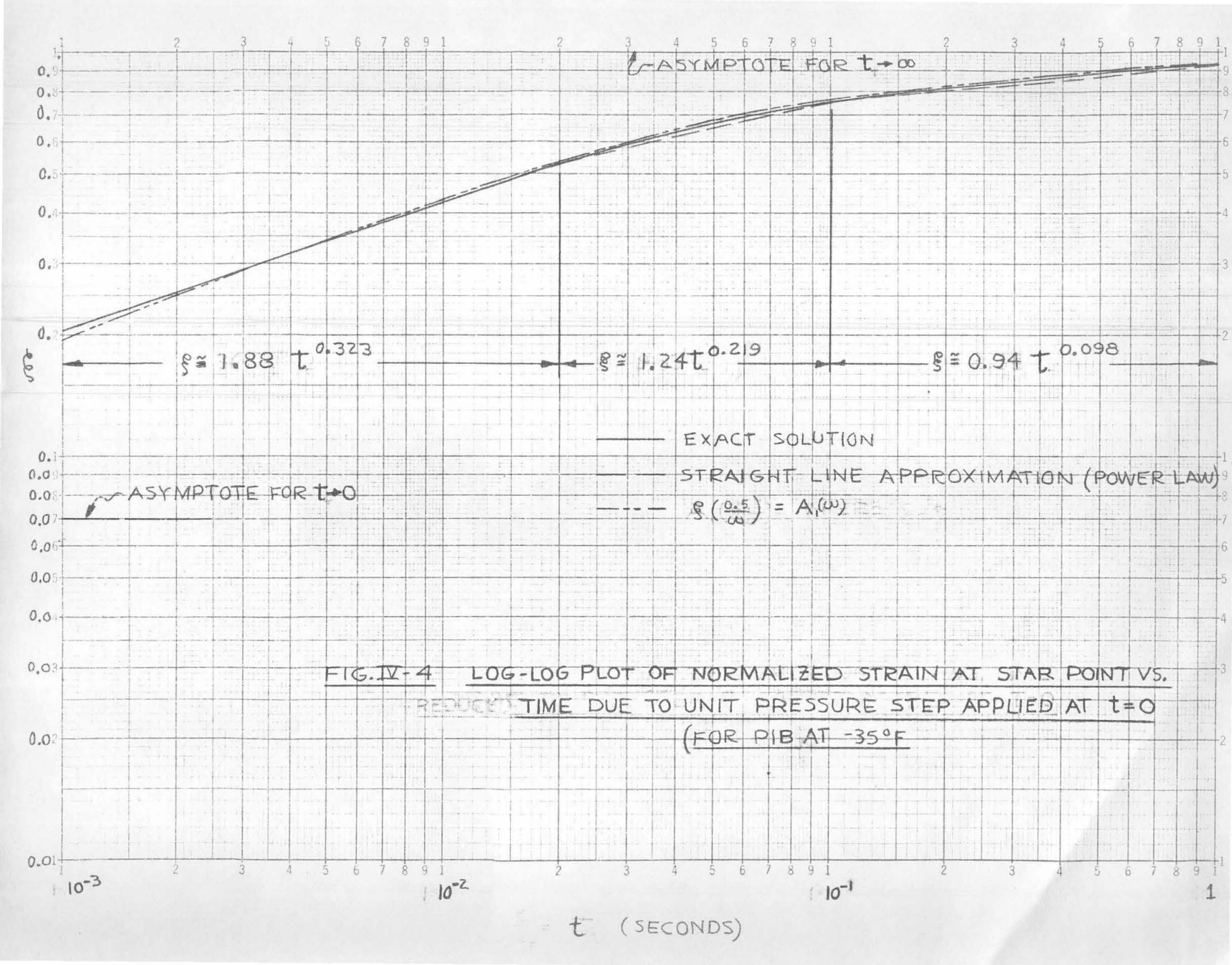

FIG. IV-4 LOG-LOG PLOT OF NORMALIZED STRAIN AT STAR POINT VS. TIME DUE TO UNIT PRESSURE STEP APPLIED AT t=0 (FOR PIB AT -35°F

REFERENCES

1. A. V. Tobolsky, "Stress Relaxation Studies of the Viscoelastic Properties of Polymers", Journal of Applied Physics, Vol. 27, p. 673, July 1956.

1* On page 697 of cited reference, the stress relaxation integral is written as $E_{rel} = \int_{-\infty}^{\infty} H(\ln\tau) e^{-t/\tau} d\ln\tau$. It is formally correct to express the limits as if the integral is of the Stieltje type of the independent variable T, and not of d lnτ; thus:

$$E_{rel} = \int_{0}^{\infty} H(\ln\tau) e^{-t/\tau} d\ln\tau = \int_{-\infty}^{\infty} H(\zeta) e^{-te^{-\zeta}} d\zeta$$ is better.

2. P. J. Blatz, "The Rheology of Composite Solid Propellants", Industrial Engineering Chemistry, Vol. 48, p. 727 (1956).

3. Widder, Laplace Transform

4. ibid

5. R. Cole, Journal Chemical Physics, Vol. 18, p. 1417 (1950).

6. Williams, Landel, Ferry, Journal of American Chemical Society, Vol. 77, p. 370, (1950).

7. R. Cole, Journal Chemical Physics, Vol. 18, p. 443, (1950).

8. R. F. Landel, Trans Soc. Rheology II, p 53 (1958).

9. Landel, Smith, External Publication No. 655, Jet Propulsion Laboratory, California Institute of Technology.

10. R. A. Schapery, L. D. Stimpson, M. L. Williams: "Fundamental Studies Relating to Systems Analysis of Solid Propellants", California Institute of Technology GALCIT 101, Progress Report No. 1, January 15, 1959.

11. R. A. Schapery, L. D. Stimpson, M. L. Williams: "Fundamental Studies Relating to Systems Analysis of Solid Propellants", California Institute of Technology GALCIT 101, Progress Report No. 2, April 15, 1959.

12. R. A. Schapery, L. D. Stimpson, M. L. Williams: "Fundamental Studies Relating to Systems Analysis of Solid Propellants", California Institute of Technology GALCIT 101, Progress Report No. 3, July 15, 1959.

13. R. A. Schapery, L. D. Stimpson, M. L. Williams: "Fundamental Studies Relating to Systems Analysis of Solid Propellants", California Institute of Technology GALCIT 101, Progress Report No. 4, October 15, 1959.

14. H.Leaderman, Trans. Soc. Rheology, Vol. 1, p 213, (1957).

15. E. H. Lee, "Viscoelastic Stress Analysis", Brown University, NR-064-406, July 1958.

16. T. von Karman, M. A. Biot, "Mathematical Methods in Engineering", McGraw-Hill, New York, p. 333, (1940).

17. R. F. Landel, Trans. Soc. Rheology, Vol. II, pps 53-75, (1958).

18. D. R. Bland, E. H. Lee: "On Fitting a Four Element Visco-Elastic Model to Measured Complex Compliance Functions", Brown University Technical Report No. 13, NORD 11496, June 1955.

19. T. von Karman, M. A. Biot: "Mathematical Methods in Engineering", McGraw-Hill, New York, p. 403, (1940).

20. Seidman, Mitchell H.: "Stresses at Boundary of Thin Elastic Slab Imbedded in Semi-infinite Medium, Due to Pressure Normal to Free Surface (GALCIT SM 59-10) California Institute of Technology, May 1959.

DISTRIBUTION LIST

Galcit 101

GOVERNMENT AGENCIES

Advanced Research Projects Agency
Washington 25, D. C.
Attn: Mr. John Kincaid (1)

National Aeronautics and Space Administration
1512"H" Street, N. W.
Washington 25, D. C.
Attn: Mr. Elliott Mitchell (1)

National Aeronautics and Space Administration
Lewis Research Center
21000 Brookpark Road
Cleveland 35, Ohio
Attn: Mr. George Mandel (1)

Office of the Department of Defense, Research and Engineering
Pentagon Building, Room 3E1030
Washington, D. C.
Attn: Mr. William E. Sheehan (1)

Solid Propellant Information Agency
The Johns Hopkins University
Applied Physics Laboratory
8621 Georgia Avenue
Silver Springs, Maryland
Attn: Mr. M. T. Lyons (3)

ARMY

Aberdeen Proving Ground
Internal Ballistics Laboratory
Aberdeen, Maryland
Attn: Dr. John H. Frazer, Chief (1)

Office of Ordnance Research
Box C-M, Duke Station
Durham, North Carolina
Attn: Dr. James Murray (1)

Piccatiny Arsenal
Dover, New Jersey
Attn: Miss E. MacAbee (1)

Redstone Arsenal
Army Rocket and Guided Missile Agency
Huntsville, Alabama
Attn: Mr. Thomas H. Duerr (1)

NAVY

Mechanics Branch
Office of Naval Research
Washington 25, D. C.
Attn: Dr. Harold Liebowitz (1)

Special Projects Group
Bureau of Naval Weapons
Washington 25, D. C.
Attn: Mr. William Cohen (1)

U. S. Navy Ordnance Test Station
Propulsion Development Department
China Lake, California
Attn: Mr. Douglas D. Ordahl:Code 45 (1)

AIR FORCE

Air Force Ballistic Missile Development
Solid Propellant Branch
Air Force Unit Post Office
Los Angeles 45, California
Attn: Major Ralph Harned (1)

Air Research and Development Command
European Office
Library, Technical Information Office
Shell Building 47, Rue Canterstein
Brussels, Belgium
Attn: Miss Margaret P. Papesch (1)

Flight Test Rocket Development Station
Propulsion Section
Edwards Air Force Base
Muroc, California
Attn: Mr. D. A. Hart (1)
Attn: Mr. Tom Davidson (1)

Office of Scientific Research
Washington 25, D. C.
Attn: Mr. Milton Rogers (1)

Space Technology Laboratories
Solid Propellant Branch
Department of Propulsion Laboratory
5740 Arbor Vitae
Los Angeles, California
Attn: Mr. Robert Anderson (1)

Wright Air Development Division
Aeronautical Research Laboratory
Wright-Patterson Air Force Base
Dayton, Ohio
Attn: Mr. Richard B. Baird (1)

UNIVERSITIES

Brown University
Department of Applied Mathematics
Providence 12, Rhode Island
Attn: Dr. E. H. Lee (1)

California Institute of Technology
Pasadena, California
Attn: CALCIT Library (2)
Attn: JPL Library (2)

Columbia University
Department of Civil Engineering
New York 27, New York
Attn: Dr. A. M. Freudenthal (1)

Massachusetts Institute of Technology
Department of Mechanical Engineering
Cambridge 39, Massachusetts
Attn: Dr. M. E. Shank (1)

New York University
College of Engineering
New York 53, New York
Attn: Dr. George Gerard (1)
Attn: Dr. Bernard W. Shaffer (1)

Polytechnic Institute of Brooklyn
Department of Aeronautical Engineering
Brooklyn, New York
Attn: Dr. Radok (1)
Attn: Prof. F. Pohle (1)

University of Alabama
College of Engineering
University, Alabama
A Attn: Dr. William D. Jordan (1)

University of California
Department of Civil Engineering
Berkeley 4, California
Attn: Prof. Karl S. Pister (1)

INDUSTRIAL

Thiokol Chemical Corporation
Redstone Division
Huntsville, Alabama
Attn: Mr. James P. Lutz (6)
Attn: Mr. John S. Wise (2)

Thiokol Chemical Corporation
Elkton Division
Elkton, Maryland
Attn: Mr. Ernest Sizemore (2)

INDUSTRIAL - (cont'd)

Thiokol Chemical Corporation
Utah Division
Brigham City, Utah
Attn: Mr. C. S. Rogerts, Jr. (2)
Attn: Mr. John Bruggeman (1)

Thiokol Chemical Corporation
Hunter-Bristol Division
Bristol, Pennsylvania
Attn: Mr. Don Mueller (2)

Aerojet-General Corporation
P. O. Box 296
Azusa, California
Attn: Mr. William Cox (1)
Attn: Mr. Kenneth Bills (1)

Aerojet-General Corporation
Solid Propellant Rocket Plant
Sacramento, California
Attn: Mr. John Billheimer (1)
Attn: Mr. A. Fraser (1)
Attn: Dr. James H. Wiegand (1)

Astrodyne, Inc.
P. O. Box
McGregor, Texas
Attn: Mr. S. C. Britton (1)
Attn: Mr. C. C. Dugger (1)

Rocketdyne
6633 Canoga Avenue
Canoga Park, California
Attn: Mr. Frank Cramer (1)

Grand Central Rocket Co.
P. O. Box 111
Redlands, California
Attn: Mr. J. E. Fitzgerald (2)

Olin Mathieson Chemical Corporation
Internal Ballistics Section
Box 508
Marion, Illinois
Attn: Mr. Robert W. Ziem (1)

Boeing Airplane Company
P. O. Box 3707
Seattle, Washington
Attn: Mr. Len Hadlock (1)

INDUSTRIAL - (cont'd)

Douglas Aircraft Company, Inc.
3000 Ocean Park Boulevard
Santa Monica, California
Attn: Engineering Library (1)
Department A-260

Hughes Aircraft Company
Systems Development Laboratories
Culver City, California
Attn: Mr. Norman Au (1)

Hercules Powder Company
Allegheny Ballistics Laboratory
Cumberland, Maryland
Attn: Mr. Ross H. Petty -Library (2)
Attn: Mr. James H. Thacher (1)

Poulter Laboratories
Stanford Research Institute
Menlo Park, California
Attn: Mr. W. L. Dowler (1)

GALCIT

Internal Distribution (10)

File (3)